Diploma thesis

Comparison of different strategies for cardiac magnetic resonance imaging short-axis based evaluation of right ventricular function

submitted by

Michael Erhart

Submitted in partial fulfilment
Of the Requirements for the Degree of

Doctor of Medicine
(Dr. med. univ.)

at the

Medical University of Graz

conducted at the

Department of Radiology

under the guidance of
Univ. Prof. Dr. Michael Fuchsjäger
PD DI Dr. techn. Gert Reiter

Graz, 20.06.2017

Eidesstattliche Erklärung

Ich erkläre ehrenwörtlich, dass ich die vorliegende Arbeit selbstständig und ohne fremde Hilfe verfasst habe, andere als die angegebenen Quellen nicht verwendet habe und die den benutzten Quellen wörtlich oder inhaltlich entnommenen Stellen als solche kenntlich gemacht habe.

Graz, am 20.06.2017 *Michael Erhart eh*

Preface

During my studies at the Medical University of Graz, the heart as a central organ in the human body often was the topic during various lectures.
During my fourth year, I followed the invitation to participate in a MRi-study conducted by PD DI Dr. Ursula Reiter and PD DI Dr. Gert Reiter. Aim of the study was to acquire cardiac MRi normal values of healthy young subjects. My participation in this study sparked my interest in cardiac MRi, and after taking a basic course on cardiac magnetic resonance imaging, I decided that I want to become involved further in this captivating topic. This lead to me starting the first assessment process for this very thesis and accumulated in the form that exists now.
It was a journey not without its hardships, but one I could gather myriads of precious experiences from.

Acknowledgment

First, I want to thank Univ.-Prof. Dr. Michael Fuchsjäger for the opportunity to conduct this thesis at his Department of Radiology at the Medical Univerity of Graz.
An immense gratitude goes out to PD DI Dr. Ursula Reiter and PD DI Dr. Gert Reiter for the tremendous help and never-ending patience during the long hours of segmentation and throughout the whole process of writing this thesis. I would not have been able to get it to its final form without them. I would also like to take this opportunity to thank my parents, Josef and Elisabeth as well as my whole family, for their continuing support and tremendous faith.
Last but definitely not least I want to thank my girlfriend Vanessa for her support during almost all of the time of my studies. Thank you for believing in me and for all the moments where you gave me the courage to carry on.

Zusammenfassung

Zielsetzung: Herz-Magnetresonanztomographie (MRT) erlaubt die Bestimmung rechtsventrikulärer (RV) volumetrischer Funktionsparameter durch die Segmentierung des RV in tomographischen Schnittbildern in Kurzachsenorientierung (SA), wobei die Definition der RV Basisebene häufig herausfordernd ist. Zentrale Ursache dieses Problems ist die komplexe Bewegung der Trikuspidalklappenebene, sowie die im Vergleich zum linken Ventrikel asymmetrische Geometrie des RV. Das Ziel dieser Studie war die Ableitung und der Vergleich funktioneller RV Normalwerte unter Verwendung verschiedener Methoden zur Definition der RV Basisebene und die Untersuchung der Konsistenz der unterschiedlichen RV Schlagvolumina (RVSV) mit den entsprechenden Schlagvolumina des linken Ventrikels (LVSV).

Material und Methoden: Zur Datenakquisition wurden 40 gesunde Probanden mittels EKG-getriggerter 1.5T MRT untersucht. Dabei wurde der gesamte linke und rechte Ventrikel mit Cine-Schnittbildstapel in Kurzachsenorientierung (SA) abgebildet. Die volumetrische Funktion des linken Ventrikels wurde durch automatische Segmentierung mittels Standardsoftware ausgewertet. RV Volumina (enddiastolisches und endsystolisches Volumen), RVSV sowie die RV Auswurffraktion wurden durch manuelle Segmentierung des RV in Enddiastole und Endsystole bestimmt. Die RV Basisebene wurde entweder direkt in den basalen SA Schnittbildern festgelegt (merged SA und SA Methode) oder durch die Position der Trikuspidalklappenebene, die in Langachsenschnittbildern (4-Kammerblick, 4CH; RV 2-Kammerblick, RV 2CH) definiert werden konnte (4CH, 4CH & RV 2CH und optimized 4CH & RV 2CH Methode) berechnet. Die volumetrischen Funktionsparameter wurden mittels t-Test, paarweiser Korrelation und Bland-Altman-Analyse verglichen.

Ergebnisse: Merged SA, SA, 4CH, 4CH & RV 2CH und optimized 4CH & RV 2CH Methode wiesen signifikante Unterschiede in allen RV Funktionsparametern auf und die 95% Limits of Agreement waren groß. Die Korrelationen der methodisch unterschiedlich ermittelten RVSV mit LVSV waren ähnlich ($r = 0.82 – 0.88$), allerdings wurde das RVSV im Vergleich zum LVSV nur bei den Methoden mit zwei langen Achsen nicht signifikant unterschätzt (LVSV = 98 ± 23 ml; 4CH & RV 2CH Methode: RVSV = 100 ± 30 ml, $p = 0.43$; optimized 4CH & RV 2CH Methode: RVSV = 102 ± 28 ml, $p = 0.06$).

Zusammenfassung: Bei der Auswertung RV volumetrischer Funktionsparameter aus SA Cine-Serien spielt die Art der Definition der RV Basisebene eine wesentliche Rolle. Bei Miteinbeziehen der langen Achsen zur Modellierung der RV Basisebene aus der Position der Trikuspidalklappe ergeben sich im Vergleich mit LVSV konsistente Ergebnisse. Die im Rahmen dieser Studie erstellten Normalwerte könnten als Referenzwerte für weitere Studien dienen.

Abstract

Purpose: Cardiac magnetic resonance (CMR) imaging enables the quantification of right ventricular (RV) function from segmentation of stacks of cine short-axis (SA) images. The asymmetric RV shape and the skew motion of the tricuspid valve complicate the definition of RV base plane. The purpose of the present study was to derive and compare reference ranges for RV function parameters employing different base plane definition algorithms and to investigate the consistency of the derived RV stroke volumes (RVSV) with left ventricular stroke volumes (LVSV).

Material and Methods: ECG-gated 1.5T CMR cine imaging was performed on forty healthy volunteers. LVSV was evaluated automatically, RV volumes (enddiastolic volume and endsystolic volume), RVSV and the RV ejection fraction where derived from manual segmentation of end-diastolic and end-systolic SA images employing standard software. RV base plane was defined from SA images only (merged SA and SA methods) and from defining junction points of the tricuspid valve in 4-chamber view (4CH) and RV 2-chamber view (RV 2CH), respectively (4CH, 4CH & RV 2CH and optimized 4CH & RV 2CH methods). Results were compared pair-wise employing correlation and Bland-Altman analysis as well as t-test.

Results: RV function parameters demonstrated significant biases and large 95% limits of agreement for the comparisons between the merged SA and the SA, the SA and the 4CH, the 4CH and the 4CH & RV 2CH, and the 4CH & RV 2CH and the optimized 4CH & RV 2CH evaluation method. LVSV correlated similarly with RVSV of all evaluation methods ($r = 0.82 – 0.88$), but only the evaluation methods employing two long-axis views did not significantly underestimate RVSV (LVSV = 98 ± 23 ml; 4CH & RV 2CH method: RVSV = 100 ± 30 ml, $p = 0.43$; optimized 4CH & RV 2CH method: RVSV = 102 ± 28 ml, $p = 0.06$).

Conclusion: All RV function parameters derived from stacks of cine SA images crucially depend on the type of RV base plane definition, whereby tricuspid valve plane modelling by two long-axis views provides the most consistent results to LV volumetric evaluation. Established RV reference ranges might serve as normal values for RV volumetric function indices in future studies.

Table of Contents

Glossary and abbreviations

4CH	4-chamber view
BMI	body mass index
BSA	body-surface area
CI	cardiac index
CMR	cardiac magnetic resonance
CO	cardiac output
ECG	electrocardiography
ED	end-diastole
EDV	end-diastolic volume
EDVi	indexed EDV
EF	ejection fraction
ES	end-systole
ESV	end-systolic volume
ESV	indexed ESV
FLASH	fast low-angle shot
FOV	field of view
LA	long-axis
LV	left ventricle
mPA	main pulmonary artery
PV	pulmonary valve
RA	right atrium
RV	right ventricle
RV 2CH	right ventricular 2-chamber view
SA	short-axis
SD	standard deviation
SSFP	steady-state free precession
SV	stroke volume
SVi	indexed SV
TV	tricuspid valve

Table of figures

List of tables

1 Introduction

Due to the asymmetric shape and the complex contraction patterns of the right ventricle (RV), the assessment of RV function is challenging. Even though echocardiography is the most widely used technique for analysis of the RV, assessing the function of the RV accurately as well as quantitatively is limited by poor acoustic windows for adequate visualization of the RV cavity, as well as near field artefacts due to the anterior localization of the RV in the chest (1, 2). Cardiac magnetic resonance (CMR) imaging represents the clinical reference standard technique for assessing the RV function and mass (3, 4). In the clinical setting, functional left and right ventricular CMR parameters are acquired according to standardized guidelines (5, 6), enabling accurate and reproducible characterization of RV size and function, which is essential not only for initial assessment, but also for management of patients with myocardial infarction, chronic heart failure, pulmonary hypertension, pulmonary embolism, and congenital heart diseases (7-11). The basic anatomic and physiologic characteristics of the RV, general approaches for the assessment of RV function and the assets and challenges of the CMR based evaluation of the RV are summarized in this paragraph to show the motivation and the aim of the present diploma thesis.

1.1 Anatomy and physiology of the right ventricle

Anatomically the RV is separated into 3 regions (12): the RV inlet region (consisting of the tricuspid valve which separates the RV towards the right atrium, the chordae tendineae and papillary muscles), the trabeculated RV apical body, and the RV outflow-tract (infundibulum), which extends from the antero-superior part of the right ventricle to the pulmonary valve. In contrast to the ellipsoidal shape of the left ventricle (LV), the RV appears triangular shaped when viewed laterally (Figure 1a) and crescent shaped when viewed in cross-section (Figure 1b). Three muscular bands partition the RV: the parietal band (forming the crista supraventricularis together with the infundibular septum), the moderator band (extending from the base of the anterior papillary muscle to the apical ventricular septum), and the septomarginal band (extending inferiorly and merging with the moderator band) (Figure 1c).

The shape of the RV is also determined by the position of the intraventricular septum, which separates the right and left ventricular cavities. The intraventricular septum appears concave towards the LV in both systole and diastole under normal conditions.

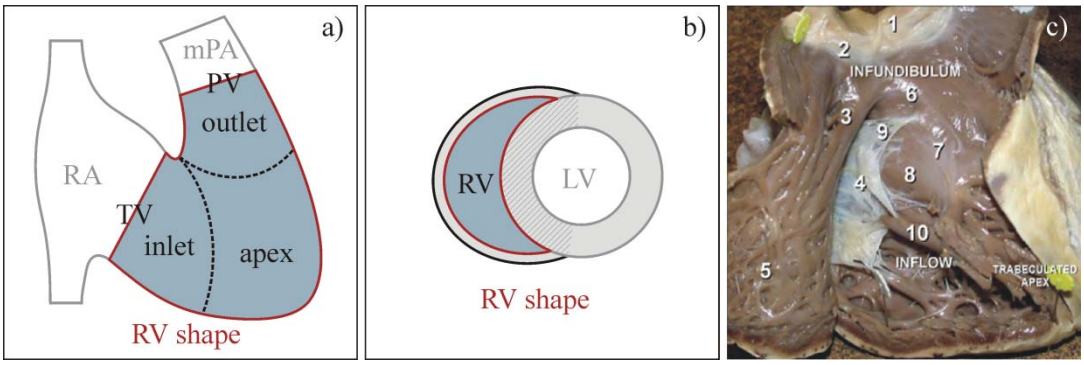

Figure 1: Normal geometry and anatomy of the right ventricle. The shape of the right ventricle (RV, red line) is triangular in lateral view a). The RV is delimited by the tricuspid valve (TV) and the pulmonary valve (PV), separating the RV cavity towards the right atrium (RA) and the main pulmonary artery (PV). Regions of RV inlet, outlet and apical body are indicated by dashed lines. Adapted from (13). Crescent shape of the RV in cross-sectional view b). The intraventricular septum (grey-shaded area) separates the RV from the left ventricular (LV) cavity. Adapted from (13). Anatomical preparation of the right heart (14) c). 1, pulmonary valve; 2, pulmonary annulus; 3, crista supraventricularis; 4, tricuspid valve; 5, right ventricular anterior wall; 6, anterior limb of trabecula septum marginals; 7 and 8, body and posterior limb of trabecula septum marginalis; 9, medial papillary muscle; 10, anterior papillary muscle.

For oxygenation, the RV pumps the blood received from the right atrium during the ventricular diastole towards the pulmonary artery and the lungs. In contrast to the LV, the RV is coupled to a low pressure, highly distensible arterial system (15). Compared to LV volumes, RV volumes are typically larger, resulting in a slightly lower RV ejection fraction (EF) (16). According to the large RV surface-to-volume ratio, smaller RV contraction provides ejection of the same blood volume per heart beat (stroke volume, SV) than the LV. Even though the myocardial wall of the RV is thin (with an end-diastolic wall thickness of 3-4 mm), the myocardial mass of the RV is about one-sixth of the LV (17). In Table 1 the major anatomical and functional differences between the right and left ventricle are summarized.

Table 1: Normal left (LV) and right (RV) ventricular structural/functional characteristics/parameters. EDV, end-diastolic volume index, EF, ejection fraction. Mass and EDV values are given normalized to the body surface area. From (15-17)

parameter	**RV**	**LV**
shape (profile/cross section)	triangle/crescent	elliptic/circular
myocardium	coarse apical trabeculation	fine apical trabeculation
wall thickness	2-5 mm	7-11 mm
mass	26 ± 5 g/m^2 [17 - 34 g/m^2]	87 ± 12 g/m^2 [64 - 109 g/m^2]
EF	61 ± 7 % [47 - 76%]	67 ± 5 % [57 - 78%]
EDV	75 ± 13 ml/m^2 [49 - 101 ml/m^2]	66 ± 12 ml/m^2 [44 - 89 ml/m^2]
filling profile	RV filling starts earlier and finishes later than the LV filling	
filling velocities	RV filling velocities are lower than LV filling velocities	
pump conditions	low resistance low capacitance	high resistance high pressure
ventricular pressure (systolic/diastolic)	25 mmHg/4 mmHg [15-30 mmHg/1-7 mmHg]	130 mmHg/8 mmHg [90-140 mmHg/5-12 mmHg]
vascular resistance	70 dyn·s·cm^{-5} [20 - 130 dyn·s·cm^{-5}]	1100 dyn·s·cm^{-5} [700 - 1600 dyn·s·cm^{-5}]

The contraction of the RV is complex and proceeds sequentially (18). RV systole starts with fast contraction of the RV inlet region, followed by the contraction of the trabeculated apex and ending with the contraction of the RV outlet (18, 19). During contraction three patterns are observed: The inward motion of the RVs free wall, the RV long axis shortening and the secondary contraction of the RV due to LV contraction translated via the intraventricular septum (Figure 2). In contrast to the LV, twisting and rotational contraction do not significantly contribute to RV contraction (20).

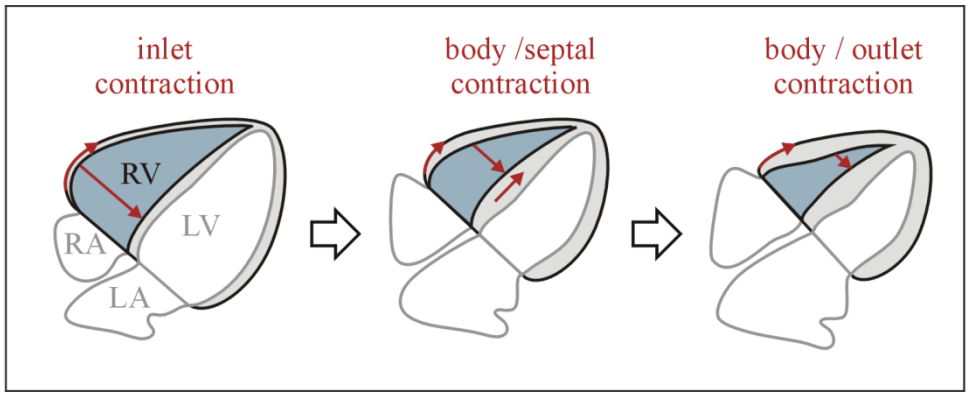

Figure 2: Right ventricular contraction patterns. Schematic drawing of the end-diastolic and end-systolic extent of the right ventricle (RV). The sequential systolic RV contraction patterns are indicated as red arrows. RA, right atrium; LA, left atrium; LV, left ventricle. Adapted from [13].

1.2 Imaging assessment of right ventricular function

Echocardiography, CMR and cardiac computed tomography have been used to capture and quantify RV function, each modality with different advantages and limitations (Table 2). Being widely available, inexpensive and save, echocardiography represents the mainstay technique for the evaluation of RV function. Quantification of the RV function by echocardiography is, however, limited by acoustic windows, dependence on operator skills, and variable image quality. To date echocardiographic evaluation of RV function is therefore mainly restricted to the measurement of linear parameters, like RV diameters, the tricuspid annular peak systolic excursion or RV fractional area change measurements (21, 22). Due to lack of geometric models for fitting RV volumes from area/lengths measurements, calculation of RV EF remains rather a method of research than clinical practice (1, 21, 23).

In contrast to echocardiography, CMR enables the accurate assessment of RV volumes and function without limitations to heart's anatomy or patients' habitus. Employing electrocardiographically (ECG) gated cine imaging, stacks of contiguous tomographic image planes covering the RV cavity provide RV volumes from adding RV endocardial areas multiplied by slice thickness throughout all slices (Simpson approach) (5). CMR parameters of volumetric function include end-diastolic (EDV) and end-systolic (ESV) volumes, stroke volume (SV = EDV-ESV), ejection fraction (EF = SV/EDV) and cardiac output (CO = SV×HF).

Age- and sex-matched normal ranges of RV volumetric parameters are typically indexed to the body-surface area (BSA), which can be estimated from a patient's height and weight by various formulas (24), e.g. the Mosteller formula BSA = (weight (kg) × height (cm)/3600)^{½} or the DuBois formula BSA = (weight (kg)$^{0.425}$ × height (cm)$^{0.725}$) × 0.007184.

Due to the high accuracy and reproducibility of parameter, CMR is the recommended reference standard technique for quantitative RV assessment (18, 22, 25, 26). Availability, costs, and long investigation times are to date the main limitations of CMR. For patients with contraindications for CMR (e.g. in-compliant electronic or metal implants, claustrophobia) cardiac computed tomography has been reported as accurate alternative for volumetric evaluation of the RV (27). The need of ionizing radiation and iodine contrast agents, however, limits the use of cardiac computed tomography, especially for serial assessment of RV function.

Table 2: Imaging modalities for routine evaluation of right ventricular function. Echo, echocardiography; CMR, cardiac magnetic resonance imaging; CCT, cardiac computed tomography; +/++/+++/++++, small/moderate/high/very high advantage; -, major limitation. From (28, 29)

parameter	2D Echo	3D Echo	CMR	CT
availability	++++	++	++	+
costs	++++	++++	++	+
scan time	25-30 min	30-35 min	40-60 min	10-15 min
temporal resolution	+++	++	++	+
spatial resolution	+++	++	+++	++++
3D acquisition	-	+++	+++	+++
real-time imaging	-	++++	+++	-
RV wall thickness	+++	+++	+++	+++
RV diameters	++	+++	++++	++++
accuracy RV volume	-	+++	++++	++++
accuracy RV EF	-	+++	++++	++++
RV mechanics	+++	+	++++	+++
tissue characterization	-	-	+++	++
radiation exposure	+++	+++	+++	-
contrast agent	+++	+++	+++	-

1.3 CMR assessment of right ventricular function

As demonstrated in Table 2, CMR allows accurate, comprehensive evaluation of RV size and function. Current guidelines (5) recommend the assessment of RV volumetric function from stacks of ECG-gated cine series covering the RV cavity in short- or long-axis orientation (Figure 3). To avoid motion artefacts, measurements are typically acquired during breath-holding.

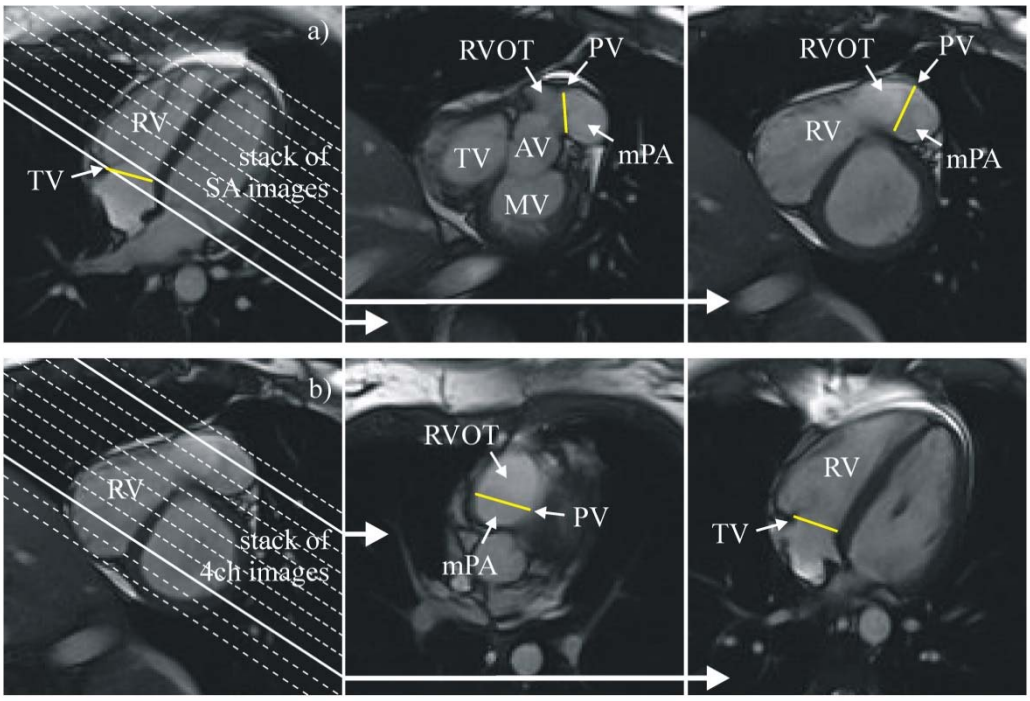

Figure 3: CMR imaging of the right ventricle (RV) using steady-state free precession (SSFP) sequence technique. A stack of images (slice thickness 6-8 mm) in short-axis (SA) (a) and long-axis (LA) (b) orientation displayed on the 4CH and a basal short-axis image, respectively. Due to the asymmetric shape of the RV, the definition of the RV cavity is challenging in basal short-axis slices, where RV inlet and outlet region typically present as separate regions. In tomographic long-axis images tricuspid (TV) and pulmonary (PV) valves clearly separate the RV from the right atrium (RA) and main pulmonary artery (mPA). RVOT, right ventricular outflow-tract (RVOT); AV, aortic valve; MV, mitral valve. CMR images of a healthy volunteer assessed at 1.5T Magnetom Sonata, Department of Radiology, Division of General Radiology, Medical University of Graz.

Besides the correct choice and adaption of the CMR sequences parameters and protocols, the precise assignment of the RV end-diastolic and end-systolic cardiac phases, agreement on rules how to delineate papillary muscles and trabeculae, and the correct definition of the RV base is crucial for the accurate and reproducible assessment volumetric functional parameters (5).

1.3.1 CMR sequence parameters and protocols for functional assessment of the RV

For assessment of ventricular function two imaging sequence techniques can be employed: ECG-gated fast low-angle shot (FLASH) or steady-state free precession (SSFP) sequence technique. Comparing FLASH and SSFP imaging for volumetric assessment of the RV, FLASH acquisition is limited by lower contrast between blood and myocardium, especially along the trabeculated endocardial RV borders (Figure 4).

In healthy subjects, RV EDV and ESV derived from FLASH protocols are smaller, resulting in larger EF but similar SV from FLASH compared to SSFP imaging (30). Age- and sex-specific reference normal values have been published for both, FLASH (16, 31) and SSFP (32-35) protocols.

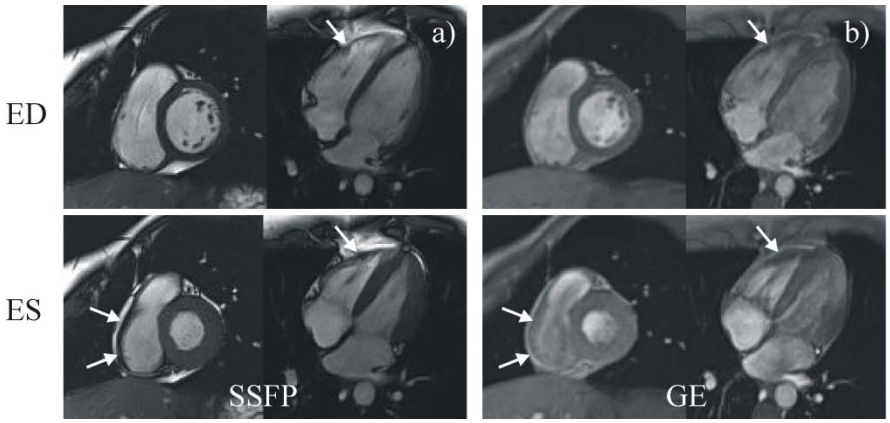

Figure 4: Fast low-angle shot (FLASH) and steady-state free precession (SSFP) imaging. SSFP images have higher signal-to-noise and contrast-to-noise ratios, providing a better definition of endocardial borders and cardiac valves. Papillary muscle and trabeculae (indicated with arrows) can be clearly identified in SSFP images in end-diastole (ED) as well as end-systole, in FLASH images separation of muscular structures in the blood pool is limited. CMR images of a healthy volunteer assessed at 1.5T Magnetom Sonata, Department of Radiology, Division of General Radiology, Medical University of Graz.

RV function can be assessed from image stacks of short- or long-axis images (Figure 4). Analysis of RV function from long-axis has been shown to be more robust, demonstrating better intra- and inter-observer reproducibility in various patient populations (36-39). CMR standard protocols mainly use stacks of short-axis (SA) slices for evaluation of RV and LV volumes to avoid an extended investigation time. RV parameters derived from SA and long-axis (LA) evaluation, however, do not reveal significant differences and strongly correlate (38, 40, 41).

1.3.2 Segmentation of the RV cavity in tomographic images

Standardized segmentation of the RV cavity from cine short- or long-axis image-stacks is the basic prerequisite for the accurate assessment of volumetric functional parameters. Papillary muscles and trabeculae can be included in- or excluded from the RV blood pool (Figure 5). Including papillary muscles and trabeculae in RV volumes results in larger volumes compared to excluding them, respectively.

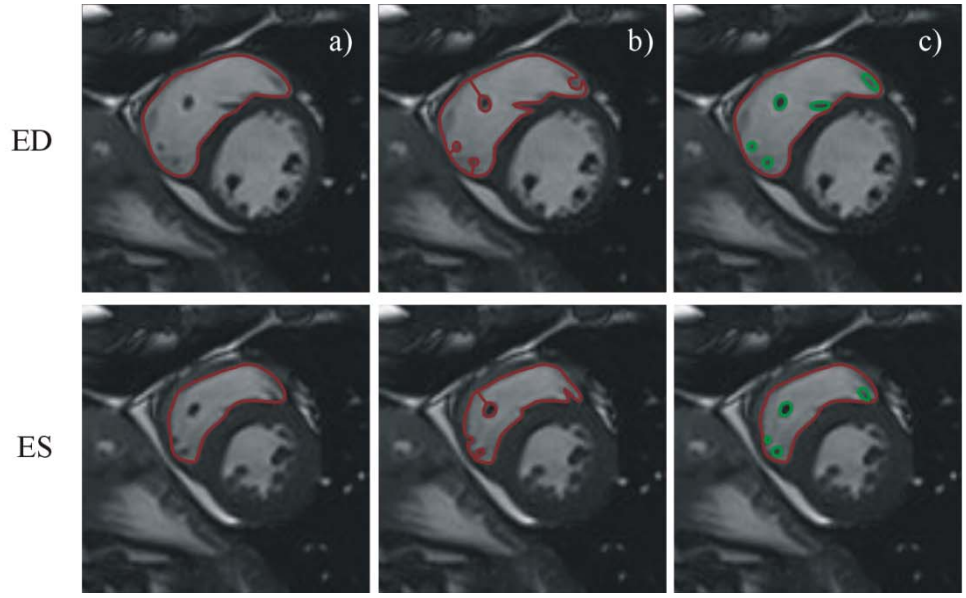

Figure 5: Segmentation methods of papillary muscles and trabeculae. Consistent delineation of the right ventricular endocardial borders (dark red) in end-diastole (ED) and end-systole (ES) is important to determine correct RV functional parameters. Papillary muscles and trabeculae can be included (a) or excluded (b) from the RV blood pool. Separate segmentation of papillary muscles and trabeculae (c) provides the possibility to subtract papillary (dark green) from ventricular volumes. Adapted from (13).

Differences between RV volumetric functional parameters including or excluding papillary muscle and trabeculae to/from RV volumes are small in healthy subjects (42) but can be large in patients with congenital heart disease (43-46). Respective reference normal values exist for both segmentation methods (32, 47). According to current guidelines papillary muscles and trabeculae should be excluded from the cavity for volume analysis and included in the myocardial mass for mass analysis (5), which – if evaluated manually – requires time-consuming segmentation.

1.3.3 Definition of the RV base plane

Due to the strong longitudinal excursion of the tricuspid valve and RV free wall during the cardiac cycle (Figure 6), the definition of the RV basal slice is crucial and contributes enormously to measured RV volumes and ejection fraction (48). In long-axis orientation the tricuspid valve plane can be clearly defined as the RV base plane throughout the cardiac cycle (Figure 3), separating the right atrium from the RV cavity. Propagating through the stack of short-axis images with the septal part of the tricuspid valve moving less than the free wall part, the RV base plane is difficult to be identified in short-axis view. Inaccurate definition of RV base plane, however, limits accuracy and reproducibility of RV volumetric functional parameters. The optimal approach for defining RV base plane is still under discussion and guidelines do not give standardized rules on what to include in the most basal planes to calculate RV volumes (5, 32, 36, 43).

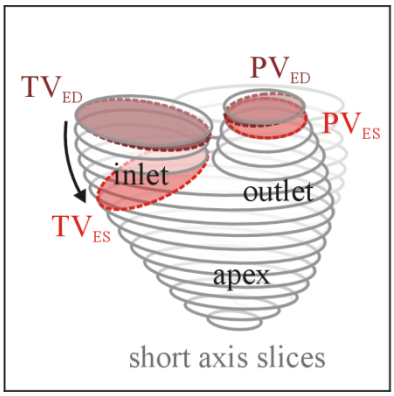

Figure 6: Schematic drawing of end-diastolic to end-systolic motion of the right ventricular (RV) base plane. The RV base plane indicated by the tricuspid (TV) and pulmonary valve (PV) planes moves through the stack of short-axis slices (gray planes). The motion is characterized by a large end-diastolic (dark red) to end-systolic (bright red) longitudinal of the RV free wall (black arrow). Adapted from (13).

To simplify the definition of the RV base plane in short-axis images, novel evaluation algorithms were recently introduced which combine the evaluation of volumetric RV data, short-axis images, and modelling of the RV of base plane from the tricuspid valve position derived from long axis images (RV 2-chamber view (RV 2CH) and 4-chamber view (4CH). The segmented RV blood-pool is retrospectively cut by the modelled plane in every cardiac phase and corrected for volumes above and below the tricuspid valve plane.

RV volumetric functional parameters using combined short-axis images for the segmentation of the RV chamber and RV long-axis images to calculate the RV base plane from tricuspid valve modelling are, however, still not available.

1.3.4 Aims of the diploma thesis

Based on the retrospective analysis of stacks of cine short-axis images and cine long-axis series acquired in healthy subjects the aims of the diploma thesis were:

- to derive reference ranges of right ventricular functional parameters employing five different base plane definitions (two short-axis only approaches and three methods employing 4-chamber and right ventricular 2-chamber view) and
- to evaluate the impact of the different right ventricular base plane definitions on the resulting right ventricular functional parameters.

Furthermore, as left and right ventricular stroke volumes should coincide in healthy subjects, left ventricular stroke volume was determined automatically from the same stacks of cine short-axis images to test the agreement with right ventricular stroke volumes derived by any of the five different base plane definitions.

2 Materials and Methods

2.1 Study population

CMR functional data of 40 young, healthy subjects (female/male, 20/20; mean age, 24 ± 4 years; age range, 19 – 38 years) without history of cardiovascular diseases or anomalies were included in the present retrospective study. These data were acquired within the study "Optimierung von nativen Herz-MR Untersuchungstechniken und Akquisition von kardialen Normalwerten bei 1.5T und 3T Magnetresonanztomographie" (EK Nr 24-126 ex 11/12). All subjects gave written informed consent. The demographic characterization of the study population is summarized in Table 3.

Table 3: Demographic characterization of the study population. Values for all subjects, females and males are given as means ± standard deviations. Numbers in the brackets indicate the range of the respective parameter [minimum, maximum]. Heart rate (HR) is the mean heart rate during functional CMR imaging. p-values refers to t-test between female and male means. BSA, body surface area; BMI, body mass index.

parameter	all	female	male	p
number	40	20	20	
age (years)	24 ± 4 [19, 38]	23 ± 3 [19, 34]	24 ± 4 [20, 38]	0.2029
weight (kg)	65 ± 9 [50, 85]	59 ± 6 [50, 75]	71 ± 7 [58, 85]	<0.0001
height (cm)	174 ± 7 [157, 188]	168 ± 5 [157, 180]	179 ± 5 [168, 188]	<0.0001
BSA (m^2)	1.8 ± 0,2 [1.5, 2.1]	1.7 ± 0,1 [1.5, 1.9]	1.9 ± 0.1 [1.7, 2.1]	<0.0001
HR (min^{-1})	64 ± 10 [43, 88]	65 ± 10 [51, 88]	62 ± 10 [43 - 77]	0.4476
BMI (kg/m^2)	21 ± 2 [18, 25]	21 ± 2 [18, 24]	22 ± 1 [19, 25]	0.0049

The body surface area (BSA) and the body mass index (BMI) were calculated from height and weight using the DuBois formula BSA (m^2) = 0.007148 × height (in cm)$^{0.725}$ × weight (in kg)$^{0.425}$ (24), the BMI according to BMI (kg/m^2) = weight (kg) / height^2 $(m)^2$, respectively.

2.2 CMR imaging

CMR imaging was performed on a 1.5T scanner (Magnetom Espree, Siemens, Erlangen, Germany) with subjects positioned in the supine position using a phased array 6-channel body matrix and a spine matrix coil. Functional cine series in cardiac long-axis and short-axis orientations (5, 6) were acquired using retrospectively ECG-gated steady-state free-precession (SSFP) cine sequences during breath-hold in inspiration.

Cine series in long-axis orientation comprised series in 4CH, LV 2-chamber view and RV 2CH (Figure 7). Protocol parameters were echo spacing = 2.9 ms, echo time TE = 1.2 ms, flip angle = 67°, measured temporal resolution TR = 44 ms reconstructed to 25 cardiac phases, field-of-view (FOV) = 315–360 × 360 mm^2 adapted to the body habitus, voxel size = 1.9 × 1.4 × 6.0 mm^3, and imaging time = 11 – 14 heart beats.

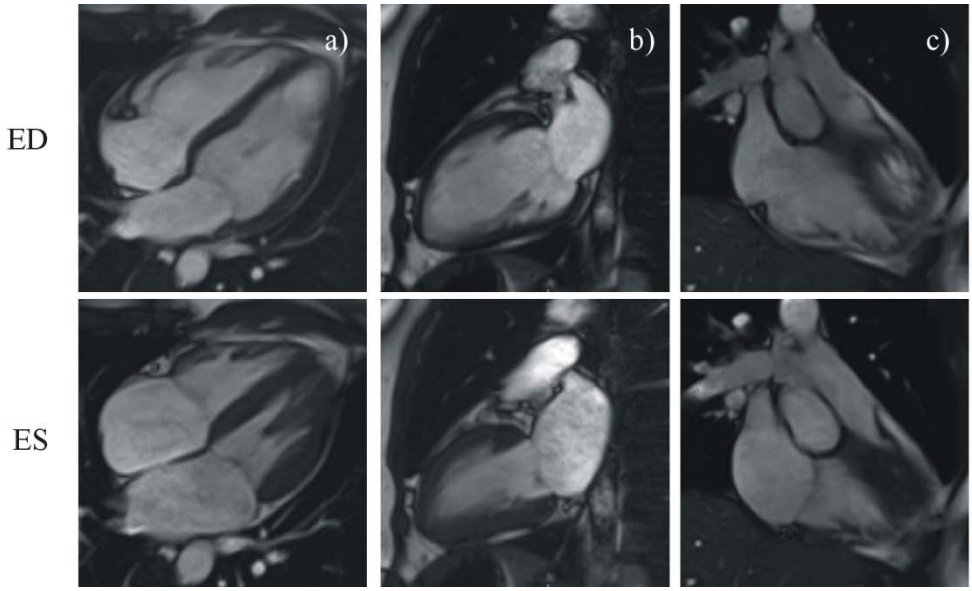

Figure 7: Typical example of cine series in long-axis orientations. 4CH (a), LV 2-chamber view (b) and RV 2CH (c) in end-diastole (ED, upper row) und end-systole (ES, lower row).

Cine series in short-axis orientation were acquired as gapless stack covering the entire left and right ventricles (Figure 8). As short-axis orientation was defined perpendicular to the intraventricular septum rather than parallel to the intra-cardiac valves, care was taken to cover the entire right ventricle throughout the whole cardiac cycle. Protocol parameters of the cine short-axis series were echo spacing = 2.9 ms, echo time TE = 1.2 ms, flip angle = 67–72°, measured temporal resolution TR = 40–51 ms reconstructed to 25 cardiac phases, field-of-view FOV = 236–315 × 360 mm^2 adapted to the body habitus, voxel size = 2.2 × 1.4 × 8.0 mm^3, and imaging time = 6 – 10 heart beats. Typically, two slices were acquired within one breath-hold interval.

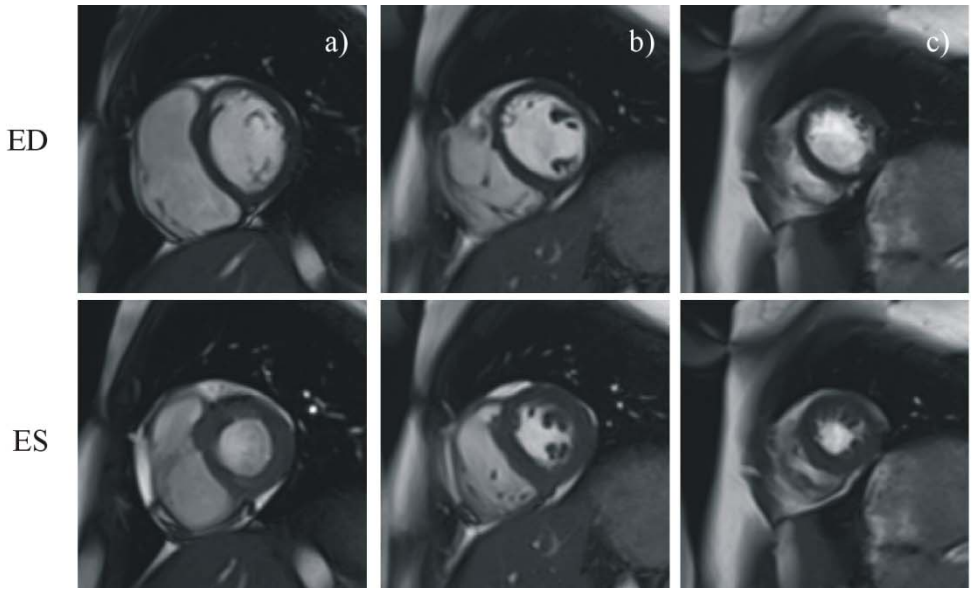

Figure 8: Typical example of cine series in short-axis orientations. Basal (a), mid-ventricular (b) and apical (c) short-axis image in end-diastole (ED, upper row) und end-systole (ES, lower row).

2.3 Determination of right ventricular functional parameters

Quantification of volumetric right ventricular functional parameters based on the Simpson approach was done by utilizing dedicated cardiac software (syngo.via software version VA30, Siemens, Erlangen, Germany). Volumetric assessment of the right ventricular cavity was derived either from the stack of cine short-axis images only, or from short-axis cine images together with long-axis slices (4CH and RV 2CH) to define the double-oblique tri-cuspid valvular plane as base of the right ventricle.

The following paragraphs summarize the data evaluation process resulting in five different base plane definitions with different RV EDV, ESV, SV, EF, and CO.

Previous to the segmentation of the right ventricular cavity end-diastolic and end-systolic time-frames were assigned. These cardiac phases were determined from visual inspection of the right ventricular lumen in a mid-ventricular short-axis slice: The end-diastole was identified as the time-frame with its largest extension (which coincided in all cases with the first time-frame representing the time of R-wave in retrospectively ECG-gated cine series), the end-systole as the time-frame with its smallest extension. The segmentation of the right ventricular cavity was performed manually in end-diastole and end-systole. Papillary muscles and trabeculae were considered as part of the inter-ventricular blood pool and therefore included to the cavity in all slices (Figure 9).

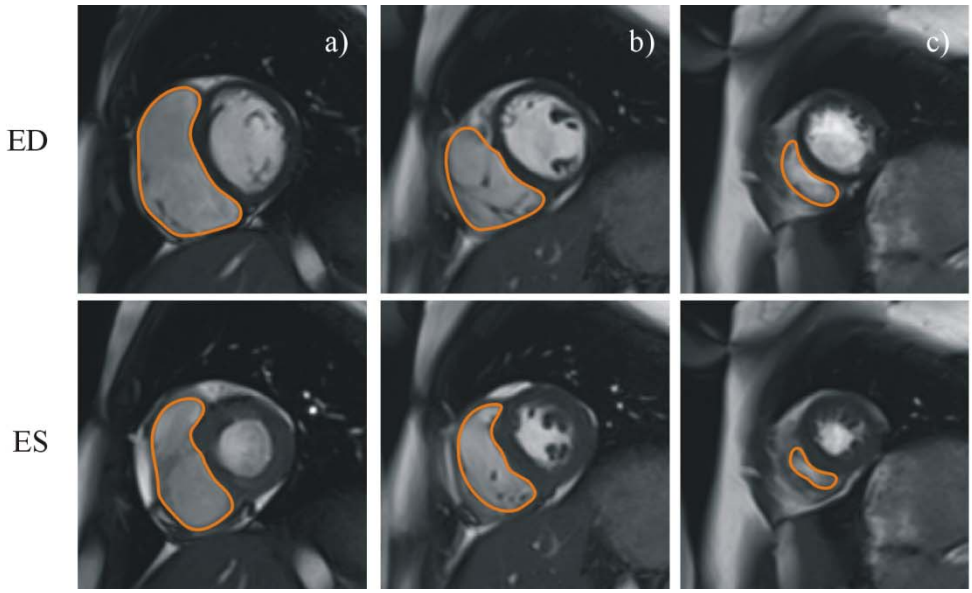

Figure 9: Typical delineation of the right ventricular cavity on short-axis images. Basal (a), mid-ventricular (b) and apical (c) short-axis image in end-diastole (upper row) und end-systole (lower row). Papillary muscles and trabeculae are considered as part of the blood pool.

Right ventricle's base was defined in different ways. When using short-axis images only, base planes coincide with most basal short-axis planes with delineated right ventricular volume. Two methods were evaluated:

- "Merged SA method": The end-diastolic and end-systolic right ventricular short-axis base plane was defined as the first slice where the right-ventricular outflow-tract and the right ventricular cavity appeared as a merged region. Areas of the right ventricular outflow-tract shown separated from the tricuspid valvular region were excluded from right ventricular short-axis volumetric evaluation (Figure 10).

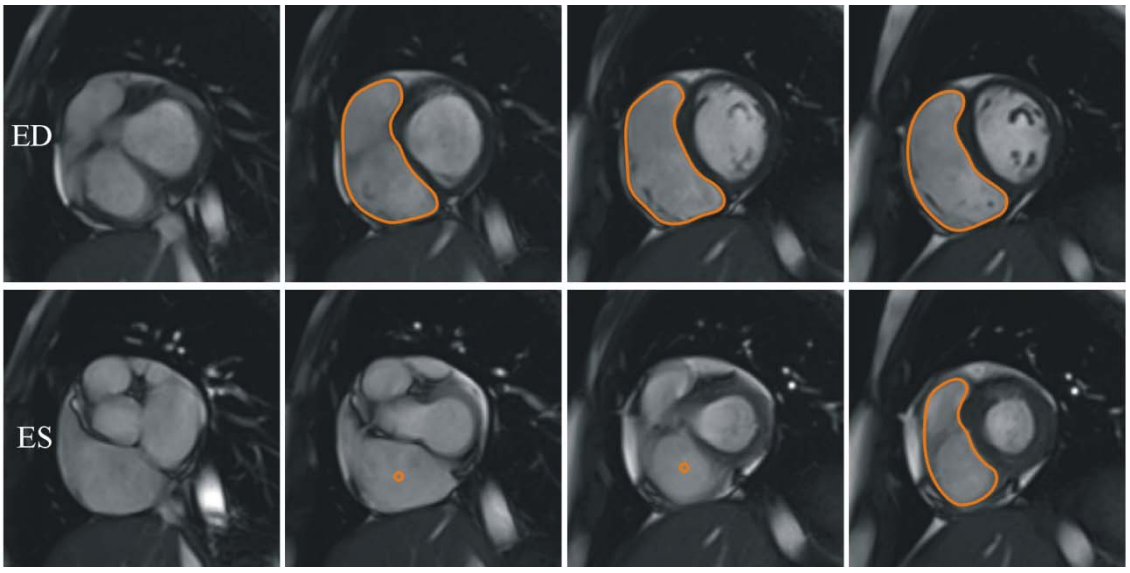

Figure 10: Typical base plane definition in the "merged SA method". Four consecutive basal short-axis images in end-diastole (upper row) und end-systole (lower row). End-diastolic base was defined as the second slice and end-systolic base as the fourth slice, because in the preceding slices outflow-tract and the right ventricular cavity do not appear as a merged region. The small contour in the middle systolic short-axis slice was drawn as a workaround, because the employed software does not allow excluding slices in specific cardiac phases.

- Normal "SA method": Compared to the "merged SA method" additional basal short-axis slices were segmented and counted to the right ventricular volume if the right-ventricular outflow-tract and the right ventricular cavity appeared only separated by partial volume borders and/or the segmented regions clearly lay behind the tricuspid valve ring and in front of the pulmonary valve (Figure 11).

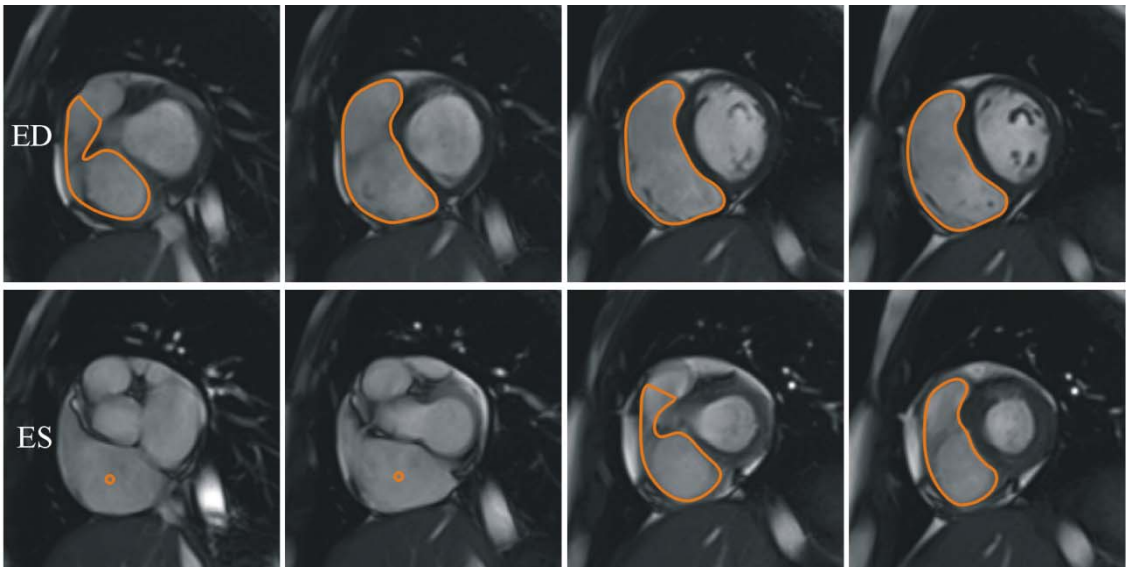

Figure 11: Typical base plane definition in the "SA method". Two consecutive basal short-axis images in end-diastole (ED, upper row) und end-systole (ES, lower row). End-diastolic base was defined as the first slice and end-systolic base as the third slice, because outflow-tract and the right ventricular cavity are separated only by partial volume borders. The small contour in the first systolic short-axis slice was drawn as workaround, because the employed software does not allow excluding slices in specific cardiac phases.

Further definitions of right ventricle's base employed either the cine images in 4CH alone or the cine images in 4CH and RV 2CH. In a first step, the delineation of right ventricular (and atrial) cavity was extended to all short-axis slices in order to account for all relevant portions of right ventricular volume that might have been cut from the initial evaluation for some reason. Then three long-axis-view-based methods of tricuspid valve plane definition and their usage as right ventricular base plane were evaluated:

- "4-chamber method": The orientation of the tricuspid plane was manually assigned by two points defining the lateral and septal atrio-ventricular junctions visualized in the 4CH, both in end-diastole and end-systole. The right ventricular base plane was modelled as a plane perpendicular to the 4-chamber orientation through the defined two points. Manually segmented volume was counted to the right ventricular volume according to its localization above or below the calculated position of the tricuspid valve plane (Figure 12).

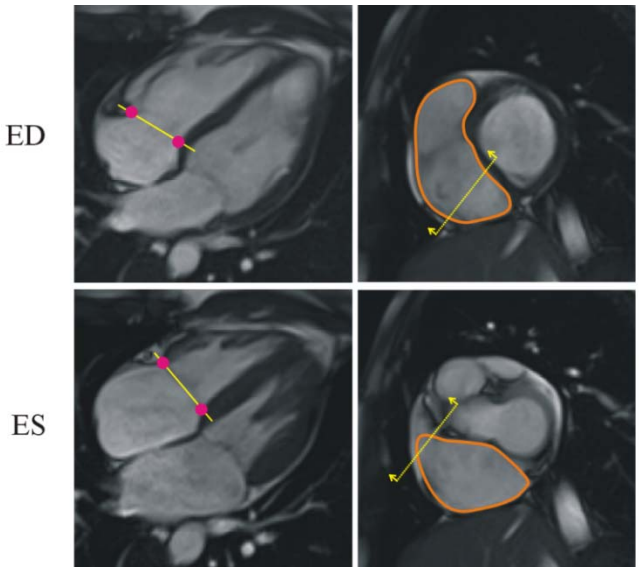

Figure 12: Typical base plane definition in the "4CH method". 4CH images (left) and basal short-axis images (right) in end-diastole (upper row) und end-systole (lower row). Markers (pink dots) were set on lateral and septal atrio-ventricular junctions of tricuspid valve in 4CH. The resulting base plane perpendicular to the 4-chamber orientation is indicated by the yellow line on 4CH and basal short-axis image as well. Yellow arrows indicate the portion of segmented volume counted to the right ventricular volume.

- "4- and RV 2-chamber method": To enable modelling an orientation of the tricuspid valve plane oblique to the 4CH, the anterior and posterior position of the valvular plane was additionally assigned in the RV 2CH. As three points define the orientation of one plane in a 3-dimensional data set, four-point modelling of a plane calculates the double-oblique orientation as best fit of a plane located closest to all four points (Figure 13).

- "Optimized 4- and RV 2-chamber method": The best fit plane that results from the markers in the junctions of the tricuspid valve in the 4CH and RV 2CH does not necessarily intersect the marker points. It might even happen that the plane does by far not represent the tricuspid valve plane indicated by the leaflets of the tricuspid valve. To compensate for this, marker points were shifted away from the junctions of the tricuspid valve until the resulting base plane showed best coincidence with tricuspid valvular plane in 4CH and RV 2CH (Figure 14).

Table 4 summarizes the different evaluation methods of RV volumetric parameters.

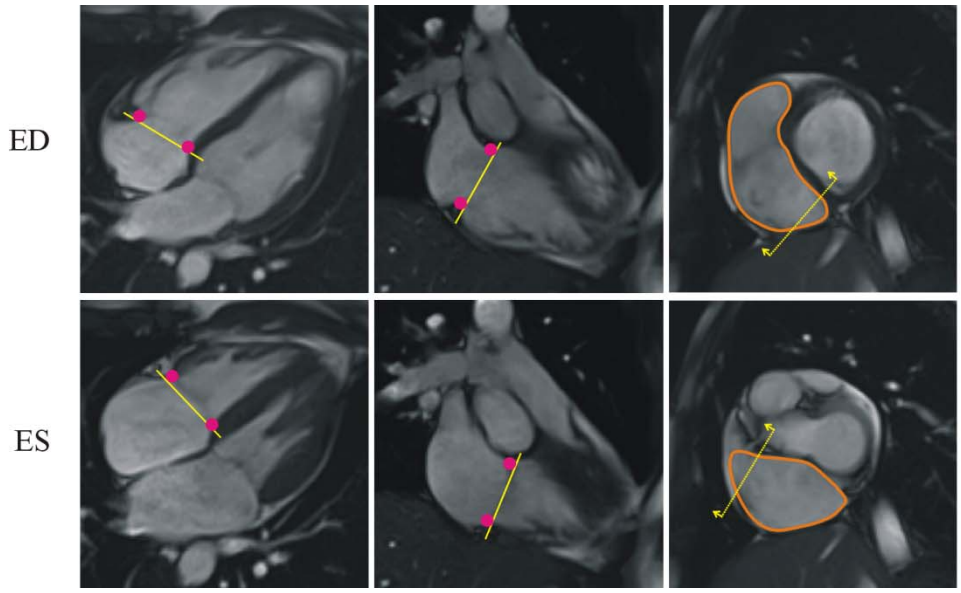

Figure 13: Typical base plane definition in the "4CH & RV 2CH method". 4CH images (left), RV 2CH images (middle) and basal short-axis images (right) in end-diastole (upper row) und end-systole (lower row). Markers (pink dots) were set on lateral and septal atrio-ventricular junctions of tricuspid valve and right ventricle in 4CH view and on the anterior and posterior junctions of tricuspid valve. The resulting base plane is indicated by the yellow line on 4CH, on RV 2CH and basal-short axis image as well. Yellow arrows indicate the portion of segmented volume counted to the right ventricular volume.

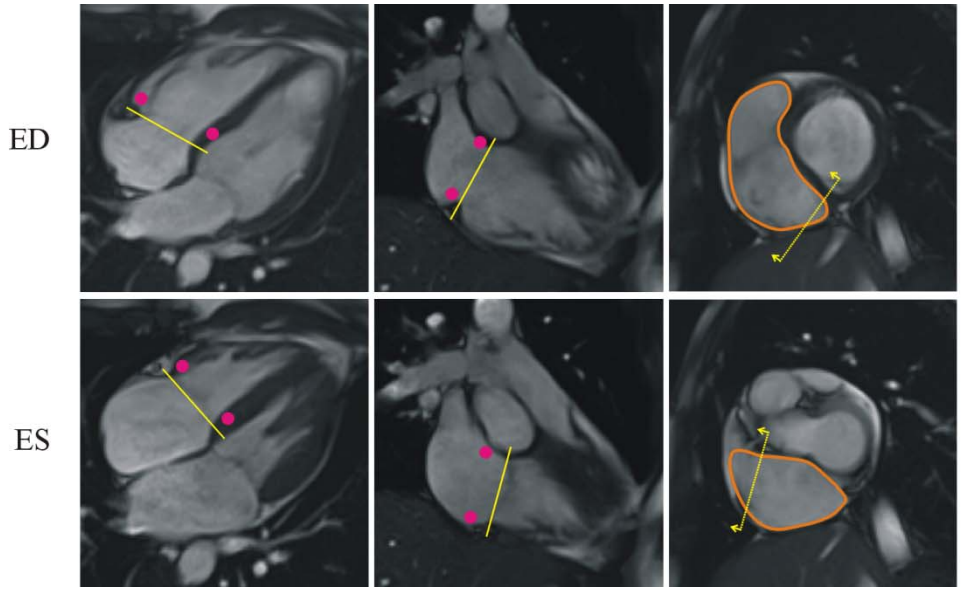

Figure 14: Typical base plane definition in the "optimized 4CH & RV 2CH method". As seen in Figure 13, where the positions of the markers are shown for the 4CH & RV 2CH method, the yellow line does not necessarily go through the markers or the perceived base plane. This figure shows the "optimized" base plane definition in end-diastole (upper row) and end-systole (lower row): Markers do not coincide with junctions of the tricuspid valve, the resulting base plane, however, (yellow lines in 4CH and RV 2CH view) describes the tricuspid valvular plane better.

Table 4: Different evaluation methods of RV volumetric parameters. SA, short-axis view; 4CH, 4-chamber view; RV-2Ch, right ventricular 2-chamber view.

method	employed cine series	base plane	derived parameters
merged SA	SA	most basal merged SA	EDV, ESV, SV, EF, CO
SA	SA	most basal SA	EDV, ESV, SV, EF, CO
4CH	SA, 4CH	junctions of tricuspid valve in 4CH	EDV, ESV, SV, EF, CO
4CH & RV 2CH	SA, 4CH, RV 2CH	junctions of tricuspid valve in 4CH & RV 2CH	EDV, ESV, SV, EF, CO
optimized 4CH & RV 2CH	SA, 4CH, RV 2CH	junctions of tricuspid valve in 4CH & RV 2CH	EDV, ESV, SV, EF, CO

2.4 Determination of left ventricular stroke volume

Additional to the derivation of RV volumetric parameters, cine series in short-axis, 4-chamber and LV 2-chamber view were employed to derive LV stroke volume (LVSV) using the same dedicated cardiac software. In contrast to the RV volumetric evaluation the software provides the segmentation of the left ventricular cavity in short-axis images, the base plane modelling via detection of mitral valvular junctions in long-axis cine images and the calculation of LV functional parameters automatically (Figure 15) (49) and LVSV values generated in this way were used without any further manual corrections.

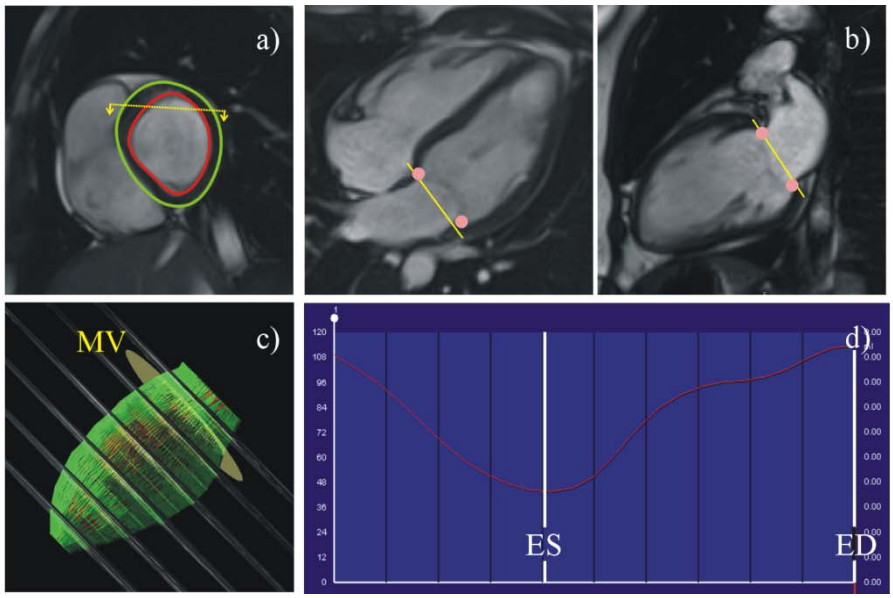

Figure 15: Typical automated determination of left ventricular stroke volume. Endo- (red) and epicardial borders (green) of the left ventricle were automatically delineated on short-axis images (a); junctions of mitral valve were automatically found (and marked by pink dots) in 4- and 2-chamber view (b). The resulting best fit base plane to the 4 junction points is indicated by the yellow line on the basal short-axis image and the two long-axis views. In combination with the segmentation of LV endocardial contours this definition of base plane resulted in the LV volume time curve (c) in all cardiac phases. LVSV is calculated as the difference between the LV enddiastolic and endsystolic volumes.

2.5 Statistical analysis

Distributions of parameter values were characterized by mean ± standard deviation (SD) and by the parameter range, where appropriate. Statistical analysis was performed with MedCalc® statistical software (version 15.11.4, MedCalc Software bvba, Ostend, Belgium 2015). A significance level of $p<0.05$ was employed for all statistical tests.

Gender-independent and gender-dependent 95% reference ranges of all right ventricular functional parameters by any of the studied evaluation methods were calculated employing the robust method suggested in Effron et al. (50). Male and female mean right ventricular functional parameters were also compared by t-test.

The results for right ventricular functional parameters derived from different evaluation methods were compared pairwise (merged SA vs. SA method, SA method vs. 4CH method, 4CH method vs. 4CH & RV 2CH method, and 4CH & RV 2CH method vs. optimized 4CH & RV 2CH method) utilizing correlation and Bland-Altman analysis. Pearson's correlation coefficient, bias, standard deviation of the differences, as well as 95% upper and lower limits of agreement are specified. T-test was used to test the significance of the bias. Similarly, these techniques were employed to analyse the coincidence of SV derived by any of the right ventricular evaluation methods with the automatically calculated LVSV.

3 Results

Right ventricular functional parameters and left ventricular stroke volume could be derived in all but one subject, where no adequate RV 2CH view cine series was acquired. The latter case was excluded from all statistical evaluations of the 4CH & RV 2CH and the optimized 4CH & RV 2CH evaluation methods.

3.1 Reference ranges of right ventricular functional parameters

Mean values, standard deviations and reference ranges for RV functional parameters derived by merged SA, SA, 4CH, 4CH & RV 2CH, and optimized 4CH & RV 2CH evaluation method are summarized in Table 5 - Table 9.

Irrespective of the evaluation method EF did not differ between male and female subjects. All other non-normalized and normalized RV functional parameters were larger for male than for female subjects, while CI's difference did not reach statistical significance in all methods.

Table 5: Reference values for parameters of right ventricular function evaluated by the merged SA method. Values for all subjects, females and males are given as means ± standard deviations and as 95% reference ranges. The p-value refers to t-test between female and male means.

parameter	all	female	male	p
EF (%)	48 ± 7 34 - 61	48 ± 7 33 - 62	47 ± 7 32 - 61	0.5463
EDV (ml)	148 ± 36 73 - 221	120 ± 21 72 - 167	175 ± 26 120 - 229	<0.0001
ESV (ml)	78 ± 22 32 - 123	63 ± 14 32 - 94	93 ± 18 56 - 133	<0.0001
SV (ml)	70 ± 18 32 - 108	58 ± 12 30 - 84	82 ± 16 51 - 117	<0.0001
CO (l/min)	4.4 ± 1.3 1.5 - 7.2	3.7 ± 1.0 1.3 – 5.6	5.1 ± 1.2 2.5 – 7.8	0.0004
EDVi (ml/m^2)	82 ± 15 50 - 113	72 ± 11 49 - 95	92 ± 13 65 - 119	<0.0001
ESVi (ml/m^2)	43 ± 10 23 - 64	37 ± 7 22 - 54	49 ± 9 31 - 69	0.0001
SVi (ml/m^2)	39 ± 9 21 - 57	35 ± 7 20 - 49	43 ± 8 27 - 61	0.0006
CI ($l/min/m^2$)	2.5 ± 0.7 1.0 – 3.7	2.2 ± 0.6 0.9 – 3.4	2.7 ± 0.6 1.3 – 4.1	0.0233

Table 6: Reference values for parameters of right ventricular function evaluated by the SA method. Values for all subjects, females and males are given as means ± standard deviations and as 95% reference ranges. The p-value refers to t-test between female and male means.

parameter	all	female	male	p
EF (%)	50 ± 6 37 - 63	52 ± 5 41 - 63	48 ± 7 32 - 62	0.0507
EDV (ml)	179 ± 41 88 - 259	148 ± 19 105 - 188	210 ± 34 133 - 284	<0.0001
ESV (ml)	90 ± 27 29 - 142	71 ± 13 43 - 98	109 ± 24 49 - 153	<0.0001
SV (ml)	89 ± 21 39 - 130	77 ± 12 50 - 101	101 ± 22 51 - 145	0.0002
CO (l/min)	5.6 ± 1.5 2.4 - 8.4	5.0 ± 1.1 2.4 - 7.3	6.2 ± 1.6 2.7 – 9.4	0.0062
EDVi (ml/m^2)	100 ± 17 62 - 133	89 ± 9 69 - 109	111 ± 17 75 - 146	<0.0001
ESVi (ml/m^2)	50 ± 12 23 - 72	43 ± 7 28 - 57	58 ± 12 29 - 83	<0.0001
SVi (ml/m^2)	50 ± 9 29 - 67	46 ± 6 34 - 60	53 ± 11 28 - 76	0.0224
CI (l/min/m^2)	3.1 ± 0.7 1.6 – 4.5	3.0 ± 0.6 1.6 – 4.3	3.3 ± 0.8 1.6 – 4.9	0.2103

Table 7: Reference values for parameters of right ventricular function evaluated by the 4CH method. Values for all subjects, females and males are given as means ± standard deviations and as 95% reference ranges. The p-value refers to t-test between female and male means.

parameter	all	female	male	p
EF (%)	52 ± 6 39 - 65	53 ± 6 40 - 65	51 ± 7 37 - 66	0.4154
EDV (ml)	164 ± 42 74 - 250	135 ± 28 73 - 197	192 ± 35 116 - 269	<0.0001
ESV (ml)	79 ± 22 31 - 123	64 ± 14 33 - 95	94 ± 20 51 - 134	<0.0001
SV (ml)	85 ± 24 34 - 134	71 ± 18 32 - 109	99 ± 23 51 - 150	0.0002
CO (l/min)	5.3 ± 1.6 1.9 - 8.6	4.6 ± 1.2 1.6 – 7.2	6.1 ± 1.7 2.6 –9.6	0.0021
EDVi (ml/m^2)	91 ± 19 53 - 130	81 ± 15 49 - 114	101 ± 17 66 - 137	0.0003
ESVi (ml/m^2)	44 ± 10 22 - 65	38 ± 8 21 - 56	49 ± 10 29 - 69	0.0003
SVi (ml/m^2)	47 ± 11 24 - 70	43 ± 9 22 - 63	52 ± 11 29 - 77	0.0083
CI (l/min/m^2)	3.0 ± 0.8 1.4 – 4.5	2.7 ± 0.7 1.2 – 4.2	3.2 ± 0.8 1.5 – 5.0	0.0525

Table 8: Reference values for parameters of right ventricular function evaluated by the 4CH & RV 2CH method. Values for all subjects, females and males are given as means ± standard deviations and as 95% reference ranges. The p-value refers to t-test between female and male means.

parameter	all	female	male	p
EF (%)	54 ± 6 42 - 65	56 ± 5 42 - 65	53 ± 6 42 - 67	0.5325
EDV (ml)	185 ± 50 75 - 289	151 ± 32 80 - 215	220 ± 40 130 - 312	<0.0001
ESV (ml)	85 ± 25 31 - 134	68 ± 14 39 - 98	103 ± 22 53 - 148	<0.0001
SV (ml)	100 ± 30 37 - 160	83 ± 22 30 - 127	118 ± 27 59 - 176	0.0001
CO (l/min)	6.3 ± 2.1 1.8 - 10.4	5.3 ± 1.6 0.8 – 8.2	7.3 ± 2.0 2.6 – 11.4	0.0019
EDVi (ml/m^2)	103 ± 22 55 - 148	90 ± 16 56 - 125	116 ± 21 71 - 161	0.0001
ESVi (ml/m^2)	47 ± 11 23 - 70	41 ± 8 25 - 57	54 ± 11 30 - 77	0.0001
SVi (ml/m^2)	56 ± 14 26 - 84	49 ± 11 24 - 73	62 ± 14 31 - 92	0.0031
CI ($l/min/m^2$)	3.5 ± 1.0 1.3 – 5.5	3.2 ± 0.9 0.9 – 4.9	3.9 ± 1.1 1.4 – 6.1	0.0366

Table 9: Reference values for parameters of right ventricular function evaluated by the optimized 4CH & RV 2CH method. Values for all subjects, females and males are given as means ± standard deviations and as 95% reference ranges. The p-value refers to t-test between female and male means.

parameter	all	female	male	p
EF (%)	55 ± 5 44 - 66	56 ± 5 45 - 66	54 ± 6 42 - 67	0.3859
EDV (ml)	184 ± 49 80 - 284	151 ± 30 84 - 212	219 ± 39 135 - 307	<0.0001
ESV (ml)	82 ± 24 30 - 131	66 ± 13 38 - 95	100 ± 21 52 - 145	<0.0001
SV (ml)	102 ± 28 42 - 159	85 ± 20 37 - 126	120 ± 25 67 - 174	<0.0001
CO (l/min)	6.4 ± 1.9 2.4 - 10.3	5.4 ± 1.5 1.1 – 8.2	7.4 ± 1.8 3.6 – 11.3	0.0009
EDVi (ml/m^2)	103 ± 21 57 - 146	90 ± 15 59 - 122	116 ± 20 73 - 158	<0.0001
ESVi (ml/m^2)	46 ± 11 22 - 68	40 ± 7 24 - 55	53 ± 11 29 - 75	0.0001
SVi (ml/m^2)	57 ± 13 29 - 83	51 ± 10 28 - 72	63 ± 13 35 - 91	0.0016
CI (l/min/m^2)	3.6 ± 0.9 1.7 – 5.4	3.3 ± 0.8 1.2 – 4.8	3.9 ± 0.9 1.9 – 5.9	0.0274

3.2 Comparison of SA and merged SA methods

Table 10 summarizes the methodological comparison of the merged SA evaluation method with the SA evaluation method; the corresponding Bland-Altman plots for EDV, ESV, SV and EF are shown in Figure 16.

Table 10: Comparison of right ventricular functional parameters determined by SA and merged SA method. The p-value indicates the significance of the bias. M1, evaluation method 1 = SA method; M2, evaluation method 2 = merged SA method; r, correlation coefficient; SD, standard deviation of the differences; LLoA 95% lower limit of agreement; ULoA 95% upper limit of agreement.

parameter	M1	M2	r	bias	SD	LLoA	ULoA	p
EF (%)	50 ± 6	48 ± 7	0.61	2	6	-9	14	0.0098
EDV (ml)	179 ± 41	148 ± 36	0.94	31	14	4	58	<0.0001
ESV (ml)	90 ± 27	78 ± 22	0.87	12	13	-13	38	<0.0001
SV (ml)	89 ± 21	70 ± 18	0.82	19	12	-5	42	<0.0001
CO (l/min)	5.6 ± 1.5	4.4 ± 1.3	0.87	1.2	0.7	-0.3	2.6	<0.0001
EDVi (ml/m^2)	100 ± 17	82 ± 15	0.90	17	7	3	32	<0.0001
ESVi (ml/m^2)	50 ± 12	43 ± 10	0.82	7	7	-7	20	<0.0001
SVi (ml/m^2)	50 ± 9	39 ± 8	0.74	11	7	-2	23	<0.0001
CI (l/min/m^2)	3.1 ± 0.7	2.5 ± 0.6	0.83	0.7	0.4	-0.1	1.5	<0.0001

Both mean EDV and mean ESV were substantially increased, if separated portions of the right ventricle close to the base and in the right ventricular outflow-tract were counted to the right ventricular volume. Mean increase of EDV by SA method compared to merged SA method was much larger than the mean increase of ESV, which caused significant increases of mean SV and mean EF by SA method compared to merged SA method.

As the Bland-Altman plots in Figure 16 demonstrate, EDV was increased by SA method compared to merged SA method in all but one subject, whereas ESV remained the same in many cases. Generally, however, standard deviations of differences and 95% limits of agreement of all functional parameters were rather large.

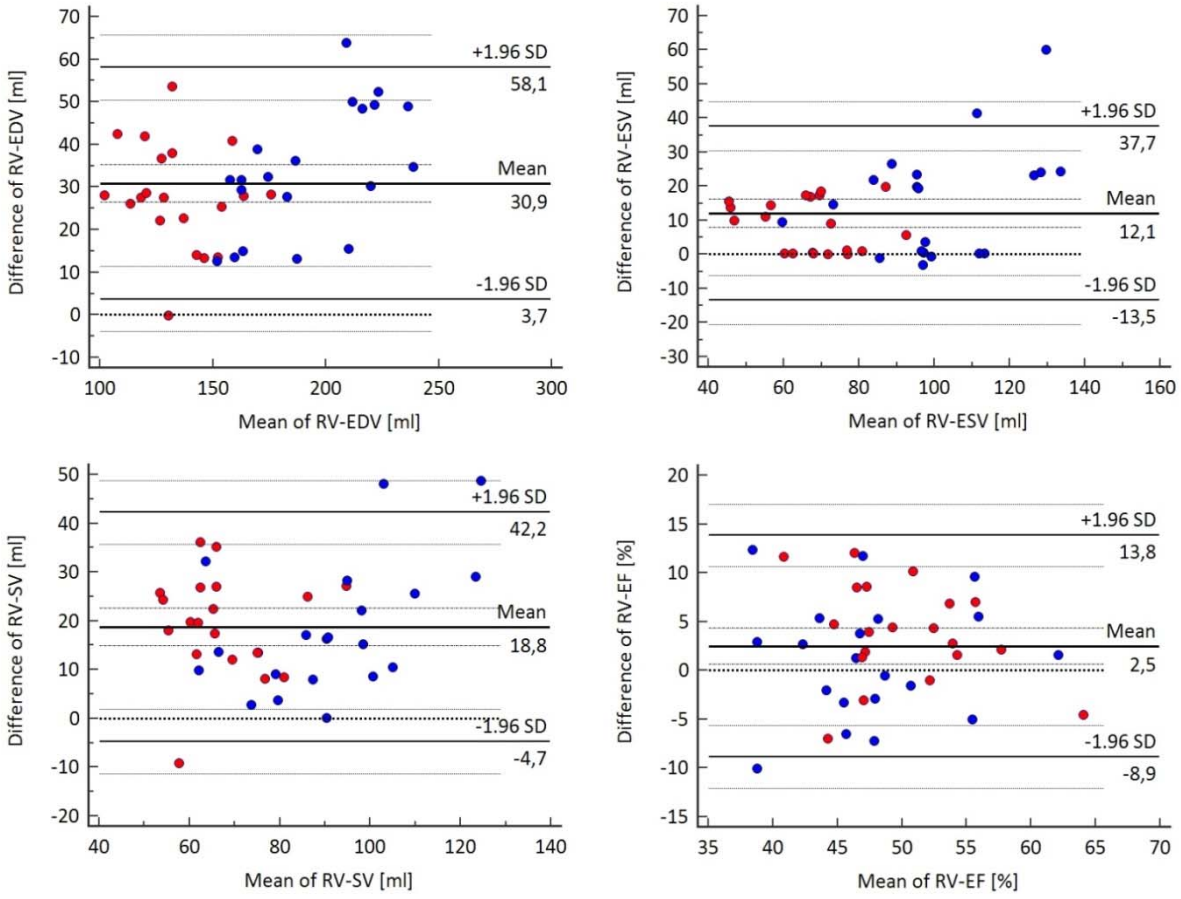

Figure 16: Bland-Altman plots comparing EDV, ESV, SV and EF determined by SA (method 1) and by merged SA methods (method 2). Blue and red dots indicate male and female subjects, respectively. SD denotes the standard deviation of differences. The thick lines indicate bias (= mean) and 95% lower/upper limits of agreement; the thin lines represent corresponding 95% confidence limits.

3.3 Comparison of SA and 4CH methods

Table 11 summarizes the methodological comparison of the long-axis based 4CH evaluation method with the SA evaluation method; the corresponding Bland-Altman plots for EDV, ESV, SV and EF are shown in Figure 17.

Table 11: Comparison of right ventricular functional parameters determined by 4CH and SA method. The p-value indicates the significance of the bias. M1, evaluation method 1 = 4CH method; M2, evaluation method 2 = SA method; r, correlation coefficient; SD, standard deviation of the differences; LLoA, 95% lower limit of agreement; ULoA, 95% upper limit of agreement.

parameter	M1	M2	r	bias	SD	LLoA	ULoA	p
EF (%)	52 ± 6	50 ± 6	0.63	2	5	-9	13	0.0427
EDV (ml)	164 ± 42	179 ± 41	0.94	-15	14	-43	13	<0.0001
ESV (ml)	79 ± 22	90 ± 27	0.90	-11	12	-35	12	<0.0001
SV (ml)	85 ± 24	89 ± 21	0.86	-4	12	-28	20	0.0533
CO (l/min)	5.3 ± 1.6	5.6 ± 1.5	0.86	-0.3	0.8	-1.9	1.4	0.0563
EDVi (ml/m^2)	91 ± 19	100 ± 17	0.90	-9	8	-25	7	<0.0001
ESVi (ml/m^2)	44 ± 10	50 ± 12	0.86	-6	6	-18	6	<0.0001
SVi (ml/m^2)	47 ± 11	50 ± 9	0.77	-2	7	-16	12	0.0404
CI (l/min/m^2)	3.0 ± 0.8	3.1 ± 0.7	0.79	0.2	0.5	-1.1	0.8	0.0421

Both mean EDV and mean ESV were substantially decreased, when the 4CH view was employed for base plane definition instead of the base plane definition by short-axis images only. The mean decreases of EDV and ESV by 4CH method compared to SA method were similar, such that mean SV and CO did not differ significantly and mean EF increased only slightly when 4-chamber evaluation method was employed.

Standard deviations of differences and 95% limits of agreement of all functional parameters were large. Moreover, Bland-Altman plots indicate a decrease of ESV differences with increasing ESV, whereas SV differences increase with increasing SV (Figure 17).

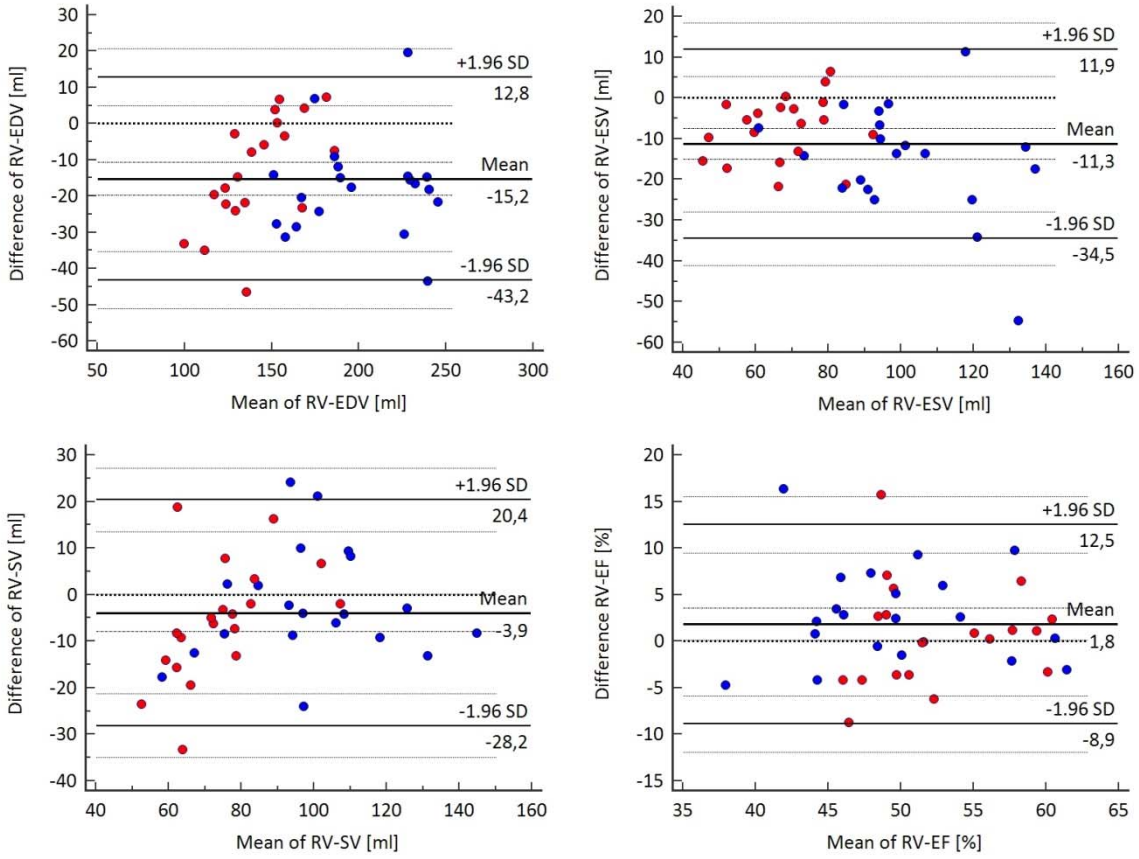

Figure 17: Bland-Altman plots comparing EDV, ESV, SV and EF determined by 4CH (method 1) and by SA methods (method 2). Blue and red dots indicate male and female subjects, respectively. SD denotes the standard deviation of differences. The thick lines indicate bias (= mean) and 95% lower/upper limits of agreement; the thin lines represent corresponding 95% confidence limits.

3.4 Comparison of 4CH and RV-2CH methods

Table 12 summarizes the methodological comparison of the 4CH evaluation method with the 4CH & RV 2CH evaluation method; the corresponding Bland-Altman plots for EDV, ESV, SV and EF are shown in Figure 18.

Table 12: Comparison of right ventricular functional parameters determined by 4CH methods with and without RV 2CH. The p-value indicates the significance of the bias. M1, evaluation method 1 = 4CH & RV 2CH method; M2, evaluation method 2 = 4CH method; r, correlation coefficient; SD, standard deviation of the differences; LLoA, 95% lower limit of agreement; ULoA, 95% upper limit of agreement.

parameter	M1	M2	r	bias	SD	LLoA	ULoA	p
EF (%)	54 ± 6	52 ± 6	0.70	2	5	-7	11	0.0114
EDV (ml)	185 ± 50	164 ± 42	0.93	22	19	-15	58	<0.0001
ESV (ml)	85 ± 25	79 ± 22	0.97	7	6	-6	19	<0.0001
SV (ml)	100 ± 30	85 ± 24	0.84	15	16	-17	47	<0.0001
CO (l/min)	6.3 ± 2.1	5.3 ± 1.6	0.86	1	1.1	-1.2	3.1	<0.0001
EDVi (ml/m^2)	103 ± 22	91 ± 19	0.90	12	10	-8	32	<0.0001
ESVi (ml/m^2)	47 ± 11	44 ± 10	0.95	4	3	-3	10	<0.0001
SVi (ml/m^2)	56 ± 14	47 ± 11	0.78	8	9	-9	26	<0.0001
CI (l/min/m^2)	3.5 ± 1.0	3.0 ± 0.8	0.82	0.5	0.6	-0.6	1.7	<0.0001

The inclusion of the RV 2CH view in the RV base plane definition increased mean EDV and ESV, the impact was, however, larger on EDV than on ESV. Both, bias and standard deviation of differences of EDV were (absolutely and relatively) larger than the one of ESV, when comparing 4CH & RV 2CH evaluation method with 4CH evaluation method. Consequently, mean SV, EF and CO were increased substantially and corresponding standard deviations of differences and 95% limits of agreement were large with the usage of a second long-axis plane for base plane definition.

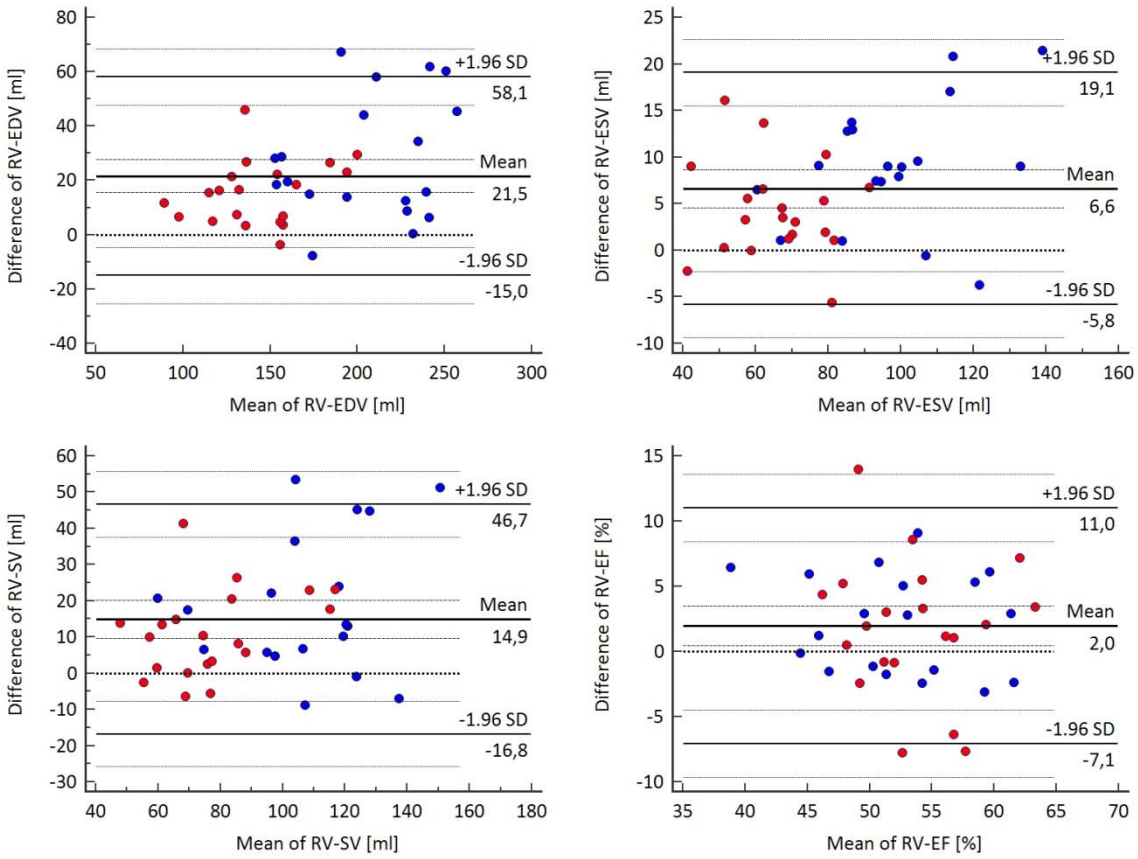

Figure 18: Bland-Altman plots comparing EDV, ESV, SV and EF determined by 4CH & RV 2CH (method 1) and by 4CH methods (method 2). Blue and red dots indicate male and female subjects, respectively. SD denotes the standard deviation of differences. The thick lines indicate bias (= mean) and 95% lower/upper limits of agreement; the thin lines represent corresponding 95% confidence limits.

3.5 Comparison of RV 2CH methods with and without base plane optimization

Table 13 summarizes the methodological comparison of the 4CH & RV 2CH evaluation method with the optimized 4CH & RV 2CH evaluation method; the corresponding Bland-Altman plots for EDV, ESV, SV and EF are shown in Figure 19.

Table 13: Comparison of right ventricular functional parameters determined by 4CH & RV 2CH methods with and without base plane optimization. The p-value indicates the significance of the bias. M1, evaluation method 1 = optimized 4CH & RV 2CH method; M2, evaluation method 2 = 4CH & RV 2CH method; r, correlation coefficient; SD, standard deviation of the differences; LLoA, 95% lower limit of agreement; ULoA, 95% upper limit of agreement.

parameter	M1	M2	r	bias	SD	LLoA	ULoA	p
EF (%)	55 ± 5	54 ± 6	0.95	1	2	-2	5	<0.0001
EDV (ml)	184 ± 49	185 ± 50	0.99	0	7	-14	13	0.7425
ESV (ml)	82 ± 24	85 ± 25	1.00	-3	2	-7	2	<0.0001
SV (ml)	102 ± 28	100 ± 30	0.97	2	7	-11	15	0.0684
CO (l/min)	6.4 ± 1.9	6.3 ± 2.1	0.98	0.1	0.4	-0.8	1	0.1449
EDVi (ml/m^2)	103 ± 21	103 ± 22	0.99	0	4	-8	7	0.7440
ESVi (ml/m^2)	46 ± 11	47 ± 11	0.99	-1	1	-4	1	<0.0001
SVi (ml/m^2)	57 ± 13	56 ± 14	0.97	1	4	-6	8	0.0626
CI (l/min/m^2)	3.6 ± 0.9	3.5 ± 1	0.97	0.1	0.2	-0.4	0.5	0.1303

Base plane optimization in case of base plane definition via 4CH and RV 2CH view resulted in smaller biases and smaller standard deviations of differences of RV functional parameters than the ones found for comparisons of other evaluation methods. However, the plane optimization caused a significant reduction in ESV and, as a consequence, a small but significant increase of EF.

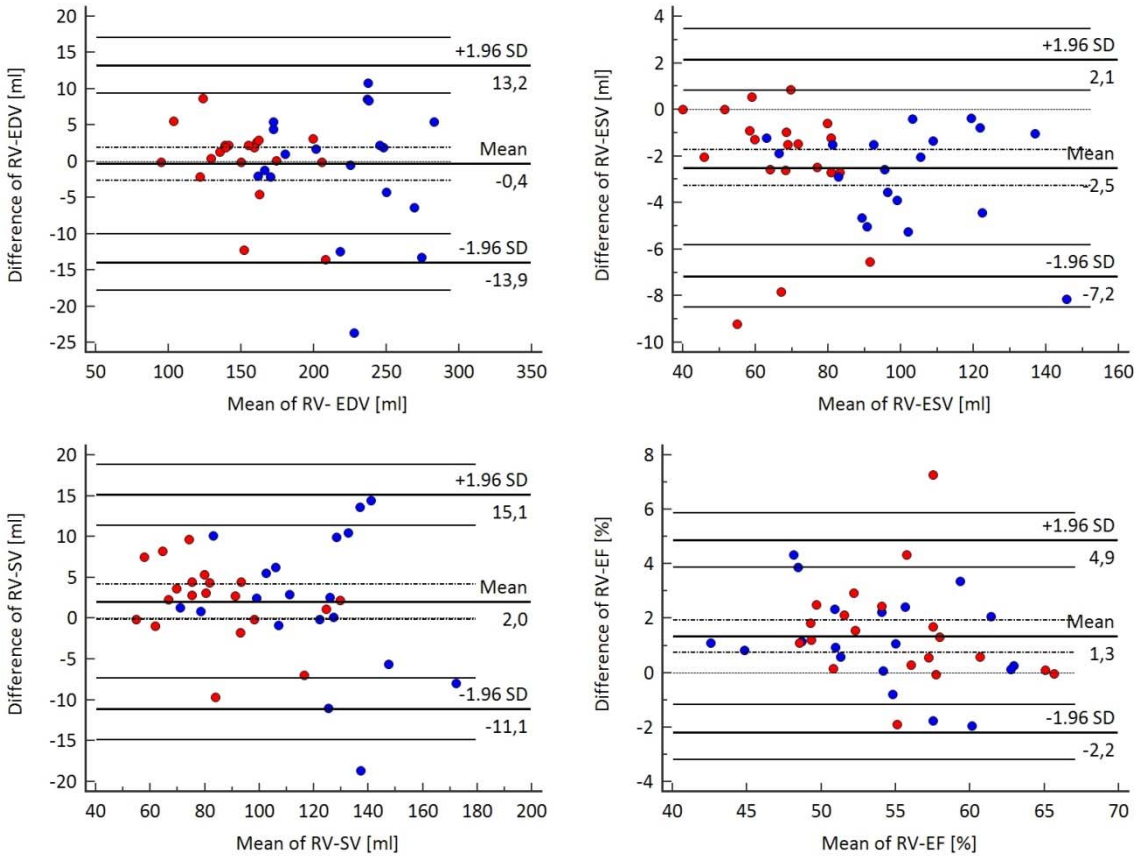

Figure 19: Bland-Altman plots comparing EDV, ESV, SV and EF determined by optimized 4- & RV 2-CH (method 1) and by 4CH & RV 2CH methods (method 2). Blue and red dots indicate male and female subjects, respectively. SD denotes the standard deviation of differences. The thick lines indicate bias (= mean) and 95% lower/upper limits of agreement; the thin lines represent corresponding 95% confidence limits**.**

3.6 Comparison of right and left ventricular stroke volumes

Table 14 summarizes the comparisons of the automatically derived left ventricular stroke volume (LVSV) with RV stroke volumes derived by the different evaluation methods; corresponding Bland-Altman plots are shown in Figure 5.

Table 14: Comparison of left ventricular stroke volume with right ventricular stroke volumes determined by different evaluation methods. The p-value indicates the significance of the bias. r, correlation coefficient; SD, standard deviation of the differences; LLoA, 95% lower limit of agreement; ULoA, 95% upper limit of agreement; LVSV, left ventricular stroke volume; RVSV, right ventricular stroke volume.

Method	RVSV (ml)	LVSV (ml)	r	bias	p	SD	LLoA	ULoA
merged SA	70 ± 18	98 ± 23	0.83	-28	<0.0001	13	-52	-3
SA	89 ± 21	98 ± 23	0.82	-9	0.0001	13	-35	17
4CH	85 ± 24	98 ± 23	0.86	-13	<0.0001	13	-38	12
4CH & RV 2CH	100 ± 30	98 ± 23	0.82	2	0.4277	17	-31	36
optimized 4CH & RV 2CH	102 ± 28	98 ± 23	0.88	4	0.0612	14	-22	31

Standard deviations of differences and correlation coefficients were similar for all RVSV evaluation methods when compared to automatically determined LVSV. The biases, however, differed: Merged SA method underestimated mean LVSV dramatically, SA and 4-chamber method underestimated mean LVSV to a lesser but significant degree and only evaluation methods employing both 4CH and RV 2CH lead to insignificant differences of mean LV and RV stroke volumes. The Bland-Altman plots of stroke volume comparisons in Figure 20 indicate that the differences between RVSV and LVSV in case of optimized 4CH & RV 2CH method tend to increase with the absolute value of stroke volume.

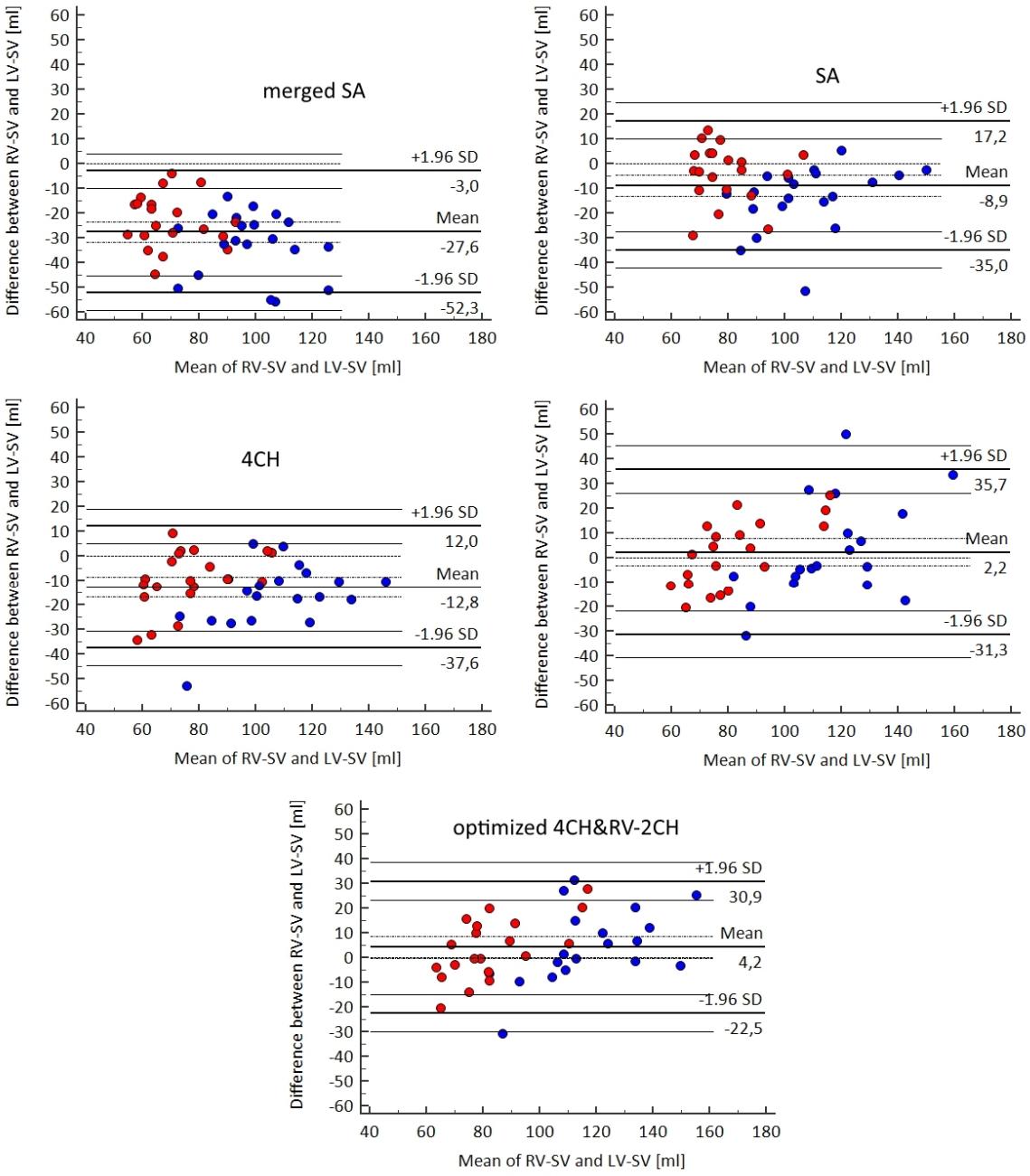

Figure 20: Bland-Altman plots comparing RVSV and LVSV. The respective evaluation method employed for determination of RVSV is indicated. Blue and red dots indicate male and female subjects, respectively. SD denotes the standard deviation of differences. The thick lines indicate bias (= mean) and 95% lower/upper limits of agreement; the thin lines represent corresponding 95% confidence limits.

4 Discussion

The current study demonstrated that all RV volumes and volumetric functional parameters assessed from cine short-axis images depend crucially on the type of RV base plane definition. Figure 21 summarizes the results for EDV, ESV, EF, CO, and SV for all RV base plane definition methods employed in the present study, as well as a comparison of the five different RVSV and the automated LVSV.

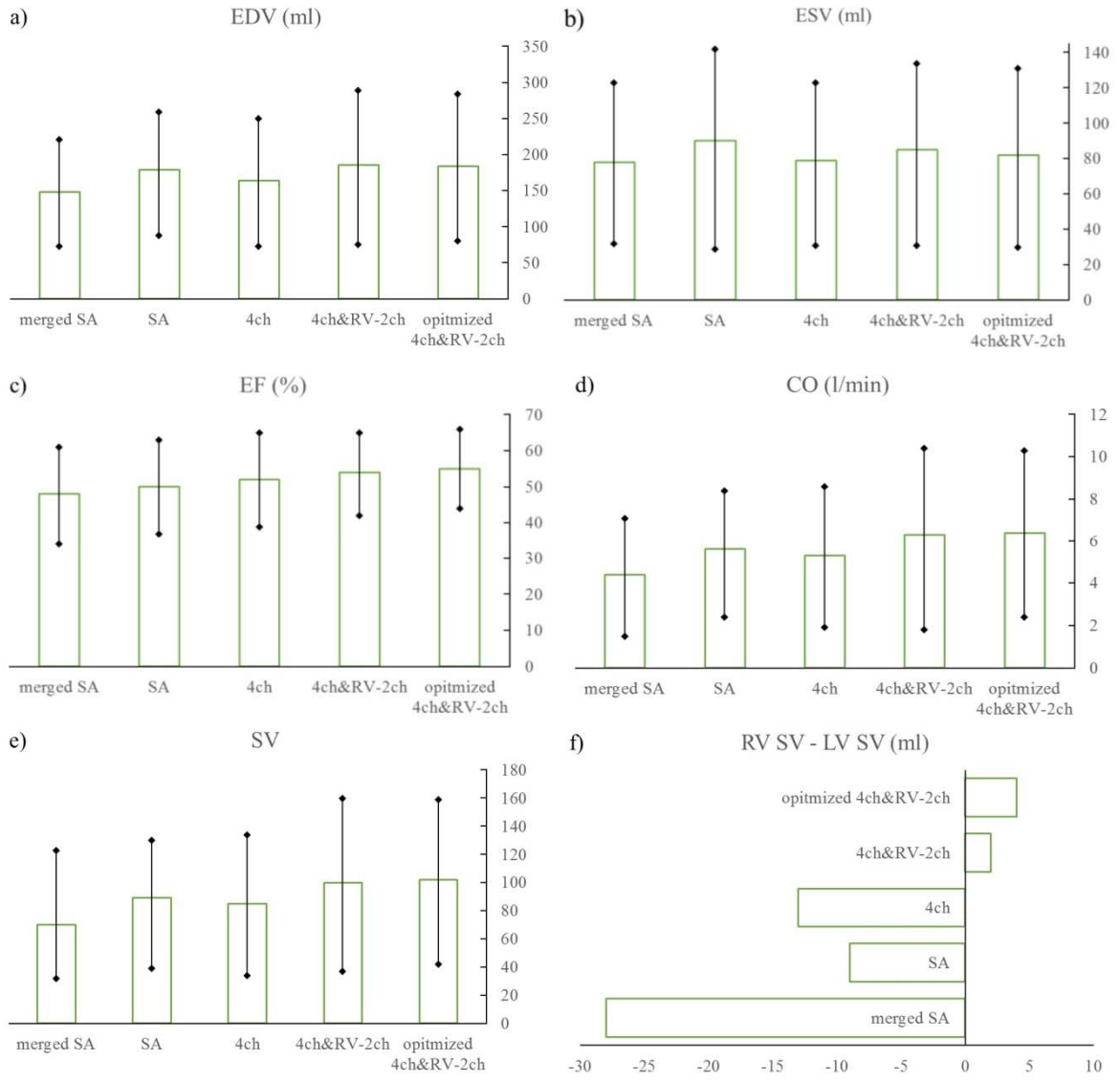

Figure 21: Comparison of derived RV volumes and functional parameters. The bars represent mean EDV (a), ESV (b), EF (c), CO (d), SV (e), and RV-to-LVSV differences (f) derived from merged SA, SA, 4CH, 4CH & RV 2CH, and optimized 4CH & RV 2CH evaluations. The black lines with diamonds indicate 95% reference ranges.

As in subjects without valvular regurgitations or shunts left and right ventricular SV calculated from respective left and right ventricular end-diastolic and end-systolic volumes equal (25), LVSV served as a reference for rating derived RV volumes suggesting base plane definition methods employing both 4-chamber and RV 2-chamber views as most consistent evaluation methods (Figure 21f).

4.1 Comparison of functional parameters derived from SA methods with literature

According to the current guidelines provided by the Society of Cardiac Magnetic Resonance for the standardized evaluation of volumetric function, the RV should be evaluated from a contiguous stack of cine SSPF short-axis (or transaxial) slices, including the right ventricular outflow-tract up to the pulmonary valve and counting RV trabeculations to the lumen of the RV cavity (5).

In the merged SA approach, the RV outflow-tract and/or RV base were not completely added to the RV cavity, as the aortic outflow-tract separates the RV at the basal level (Figure 10), resulting in a substantial underestimation of EDV, ESV and SV (as shown by the mean difference of -28 ml between RVSV and LVSV). In numerous studies, normal ranges of RV volumetric functional parameters are specified, but the detailed description of the exact segmentation procedure of the RV is often lacking (4, 16, 30, 32, 35, 36, 51, 52). Information about RV base plane segmentation can occasionally be obtained from inspection of representative figures showing the endocardial RV border. As the separated RV outflow-tract is rarely added to the RV cavity (4, 16, 30, 32, 36, 52) it can be assumed – as shown in the present study – that reported RV volumes often underestimate the size of the RV cavity.

Besides differences of RV volumes caused by the segmentation of the RV outflow tract, cine FLASH imaging for assessment of RV function (Figure 4), which was mainly used in former studies (16, 30, 36) generally provides smaller RV volumes compared to SSFP imaging due to the decreased contrast between blood and myocardium. Examples for normal ranges of the EDV and ESV reported in literature are summarized in Table 15.

Table 15: RV volume normal ranges evaluated from short-axis images from different studies.

Reference	sequence	number	RVOT yes/no	EDV (ml)	ESV (ml)
Sanstede et al. (53)	FLASH	36	no	115 ± 31	43 ± 19
Lorenz et al. (16)	FLASH	75	no	138 ± 40	54 ± 21
Matsuoka et al. (54)	FLASH	10	no	141 ± 24	57 ± 13
Grothues et al. (4)	FLASH	20	no	153 ± 34	58 ± 20
Alfakih et al. (36)	FLASH	31	no	144 ± 34	58 ± 24
Alfakih et al. (30)	SSFP	31	no	155 ± 35	68 ± 25
James et al. (38)	SSFP	30	yes	149 ± 45	
Maceira et al. (32)	SSFP	60 male	unclear	163 ± 25	57 ± 15
Maceira et al. (32)	SSFP	60 female	unclear	126 ± 21	43 ± 13
Le Ven et al. (35)	SSFP	196 male	yes	196 ± 36	75 ± 19
Le Ven et al. (35)	SSFP	238 female	yes	141 ± 24	54 ± 13
present study (merged SA)	SSFP	40	no	148 ± 36	78 ± 22
present study (SA)	SSFP	40	yes	179 ± 41	90 ± 27

In accordance with literature, RV volumes, SV and CO derived from the merged SA and SA approach in the present study significantly differed between males and females (Table 5, 6). Compared to the normal ranges of young subjects including the RV outflow-tract our results revealed comparable EDV to James et al. (38) and LeVen et al. (35), but higher ESV and lower SV for both, male and female subjects (35). Several reasons could be responsible for this discrepancy: On the one hand, the end-systolic phase was defined in a mid-ventricular short-axis slice. As the RV contraction proceeds sequentially from the inflow towards the outflow-tract (Figure 2), a basal slice would probably have resulted in a different end-systolic phase and different ESV. On the other hand, the segmentation of the trabeculated RV myocardium in end-systole is challenging due to the presence of trabeculae attached to the myocardium, limiting the definition of the endocardial border.

Moreover, window and level settings can cause major differences in the segmentation. Besides differences in the evaluation, LeVen et al. (35) acquired cine short-axis images during held end-expiration whereas in the present study subjects held the breath in shallow inspiration. Inspiratory breath-holding might alter LV and RV function (55, 56) and therefore cause differences in the measured RV volumes. Finally, in the present study subjects were fairly athletic men and women (Table 3), which could further cause differences in RV volumes obtained from other age-matched, less athletic cohorts.

4.2 RV volumes and functional parameters from long-axis based evaluations

This study is the first to report and compare normal ranges of RV volumetric functional parameters derived from cine-short axis data using RV base plane modelling via the tricuspid plane defined in 4-chamber view or a best-fit plane defined by four points in 4-chamber and RV 2-chamber view. As summarized in Figure 21, RV volumes, EF, SV, and CO derived from RV evaluation employing tricuspid valve modelling differ from RV volumes, EF, SV, and CO obtained from merged SA and SA evaluation, necessitating the definition of respective normal ranges of RV volumes and volumetric functional parameters when using any of the base plane definition algorithms mentioned above.

To define the RV base plane by the tricuspid valve plane separately from the orientation of the stack of short-axis images presents a promising approach to deal with the complex, asymmetric motion of the RV inflow tract during late systole and diastole. Calculating the base plane from two points defined by the right atrial-ventricular junctions visualized in the 4-chamber view will model a plane perpendicular to the orientation of the 4-chamber view, cutting the basal short-axis image in-plane (Figure 12). If a part of the segmented endocardial area in short-axis images is recognized to be located above the tricuspid valve, meaning in the right atrium, the respective volume is cut from the RV volume and therefore EDV and ESV are smaller than the results obtained from sole short-axis segmentation. According to RVSV-to-LVSV differences, the 4CH method presents superior results compared to the merged SA approach, and inferior to the SA method, although all three RV stroke volumes underestimate LVSV (Table 13).

This result might be caused by the fact that the tricuspid valve plane should be modelled not strictly perpendicular to the 4CH orientation throughout the cardiac cycle because this could lead to the partial inclusion of the pulmonary artery or other structures that are not part of the RV cavity and therefore cause an overestimation of the functional parameters.

To improve RV base plane modelling, the position of the tricuspid valve can be calculated as a best fit plane through the position of the septal, lateral, anterior, and inferior right atrial-ventricular junctions defined in the 4-chamber and RV 2-chamber view. Using this more realistic double oblique angulated best-fit plane as RV base plane, EDV, ESV, and SV increased compared to results derived from 4CH method, and RVSV-to-LVSV differences disappeared ($p=0.4277$). To further optimize the calculated best-fit plane, we positioned the four points in the vicinity of the RV atrial-ventricular junctions, targeting the modelled plane to exactly coincide with the tricuspid valve plane in end-diastole and end-systole (Figure 14). This optimization resulted in still insignificant ($p=0.0612$) but larger differences between RVSV and LVSV than shown in the 4CH & RV 2CH evaluation methods. However, the base plane optimization process caused significantly different ESV and EF, which might be interpreted as a heavy dependence of volumetric results on subtle changes in base plane definition points.

It is a fact that the defined plane could probably also cut the RV outflow-tract, which is a critical aspect in modelling the RV base plane as tomographic cut-plane in the 3-dimensional volume of the RV in general. Different long-axis based definitions of the base plane might easily cut different portions of the RV outflow-tract. As the inclusion of the RV outflow-tract to the RV cavity is - as recommended by current guidelines (5) but also demonstrated in the present study – essential for a correct volumetric evaluation of RV function, the relatively large standard deviations of errors between the long-axis based evaluation methods are easily understood.

4.3 Limitations

Included subjects represent a young athletic population without history and/or symptoms of cardiovascular, pulmonary or congenital heart diseases. No further blood testing, blood pressure measurement, ECG or exercise testing were performed to detect unknown cardiovascular and/or cardiopulmonary pathologies. According to the subjects' age and physical conditions, it is to be expected that the studied subjects represent RV volumetric functional parameters of healthy subjects.

Normal ranges of RV volumetric functional parameters are at present evaluated only for young male and female subjects (< 30 years). To determine age- and sex matched normal ranges for all evaluation strategies investigated within this study was out of scope of the featured diploma thesis.

An initially inexperienced observer performed the data evaluation. First data segmentations were repeated multiple times to minimize irreproducible miss-segmentation throughout the study. As data were evaluated only once by one observer, inter- and intra-observer variability of the results was not studied.

When using only short-axis images for assessment of RV volumes, the software did not allow excluding basal systolic images as drawn contours are automatically propagated throughout the cardiac phases. Therefore, small regions of interest (including some pixels) had to be drawn on systolic images to be "excluded" from volumetric evaluation. These small regions were included in the calculation of RV volumes following the Simpson approach. As these volumes were rather small (2-3 ml), they did not severely affect RV volumes evaluated via the merged SA and the SA method, but they cause a systematic overestimation of the ESV.

LVSV was evaluated by the software from automatic segmentation of LV endocardial borders. LV base plane was automatically modelled from the mitral valve plane calculated as a best fit plane using the 4-chamber and LV 2-chamber view. As shown by Harrer C (57), resulting LV volumes are reliable; however, correlations of RVSV and LVSV could possibly be improved by adapting automatic segmentation.

Segmentation of the RV cavity in short-axis images and modelling of the RV base plane via 4CH or 4CH & RV 2CH method was performed manually in the RV end-systolic and end-diastolic phase. Contours and anatomic markers were automatically propagated and corrected only if necessary. Epicardial RV contours were, however, not drawn.

Through contouring all endo- and epicardial RV contours and exact definition of anatomical markers for base plane modelling in all cardiac phases normal ranges of further RV parameters of volumetric function e.g. the RV mass, the systolic RV peak ejection rate and time, or the early and late diastolic RV peak filling rates and times could have been provided. Assessment of all data was, however, out of the scope of the diploma thesis.

4.4 Conclusion

In conclusion, the current study provides reference ranges of RV functional parameters EDV, ESV, EF, SV, and CO, including normalized values, for young healthy subjects evaluated from stacks of cine short-axis images with base planes defined either from short-axis images alone or from cine long-axis series. It could be shown that all functional parameters crucially depend on the type of RV base plane definition and that different RV base plane definitions lead to substantial biases and standard deviations for all functional parameters. Agreement on base plane definition is therefore not only important for initial assessment of RV volumetric function and reproducibility, but especially necessary when comparing individual RV volumetric function with normal ranges or to identify changes of RV volumetric parameters in follow-up investigations.

As in absence of valvular diseases and shunts consistency between RV and LV stroke volume results is desirable, base plane definition employing 4CH and RV 2CH outperformed all other RV base plane definition methods, at least when compared to long-axis based, automated LVSV determination. This result especially suggests including cine RV 2CH imaging in any functional investigation of the right ventricle as a standard procedure.

5 Literaturverzeichnis

(1) Kjaergaard J, Petersen CL, Kjaer A, Schaadt BK, Oh JK, Hassager C. Evaluation of right ventricular volume and function by 2D and 3D echocardiography compared to MRI Eur J Echocardiogr 2006;7(6):430-438.

(2) Lai WW, Gauvreau K, Rivera ES, Saleeb S, Powell AJ, Geva T. Accuracy of guideline recommendations for two-dimensional quantification of the right ventricle by echocardiography Int J Cardiovasc Imaging 2008;24(7):691-698.

(3) Pattynama PM, De Roos A, Van der Wall EE, Van Voorthuisen AE. Evaluation of cardiac function with magnetic resonance imaging Am Heart J 1994;128(3):595-607.

(4) Grothues F, Moon JC, Bellenger NG, Smith GS, Klein HU, Pennell DJ. Interstudy reproducibility of right ventricular volumes, function, and mass with cardiovascular magnetic resonance Am Heart J 2004;147(2):218-223.

(5) Schulz-Menger J, Bluemke DA, Bremerich J, Flamm SD, Fogel MA, Friedrich MG, et al. Standardized image interpretation and post processing in cardiovascular magnetic resonance: Society for Cardiovascular Magnetic Resonance (SCMR) board of trustees task force on standardized post processing J Cardiovasc Magn Reson 2013;15:35-429X-15-35.

(6) Kramer CM, Barkhausen J, Flamm SD, Kim RJ, Nagel E, Society for Cardiovascular Magnetic Resonance Board of Trustees Task Force on Standardized Protocols. Standardized cardiovascular magnetic resonance (CMR) protocols 2013 update J Cardiovasc Magn Reson 2013;15:91-429X-15-91.

(7) Hamon M, Agostini D, Le Page O, Riddell JW, Hamon M. Prognostic impact of right ventricular involvement in patients with acute myocardial infarction: meta-analysis Crit Care Med 2008;36(7):2023-2033.

(8) Ghio S, Klersy C, Magrini G, D'Armini AM, Scelsi L, Raineri C, et al. Prognostic relevance of the echocardiographic assessment of right ventricular function in patients with idiopathic pulmonary arterial hypertension Int J Cardiol 2010;140(3):272-278.

(9) Afilalo J, Flynn AW, Shimony A, Rudski LG, Agnihotri AK, Morin JF, et al. Incremental value of the preoperative echocardiogram to predict mortality and major morbidity in coronary artery bypass surgery Circulation 2013;127(3):356-364.

(10) Naeije R. Assessment of right ventricular function in pulmonary hypertension Curr Hypertens Rep 2015;17(5):35-015-0546-0.

(11) Surkova E, Muraru D, Iliceto S, Badano LP. The use of multimodality cardiovascular imaging to assess right ventricular size and function Int J Cardiol 2016;214:54-69.

(12) Ho SY, Nihoyannopoulos P. Anatomy, echocardiography, and normal right ventricular dimensions Heart 2006;92 Suppl 1:i2-13.

(13) Reiter U, Reiter C, Reiter G, Fuchsjäger M. MRT des rechten Ventrikels. [Manuscript in preparation]

(14) Haddad F, Couture P, Tousignant C, Denault AY. The right ventricle in cardiac surgery, a perioperative perspective: I. Anatomy, physiology, and assessment Anesth Analg 2009;108(2):407-421.

(15) Haddad F, Hunt SA, Rosenthal DN, Murphy DJ. Right ventricular function in cardiovascular disease, part I: Anatomy, physiology, aging, and functional assessment of the right ventricle Circulation 2008;117(11):1436-1448.

(16) Lorenz CH, Walker ES, Morgan VL, Klein SS, Graham TP,Jr. Normal human right and left ventricular mass, systolic function, and gender differences by cine magnetic resonance imaging J Cardiovasc Magn Reson 1999;1(1):7-21.

(17) Dell'Italia LJ. The right ventricle: anatomy, physiology, and clinical importance Curr Probl Cardiol 1991;16(10):653-720.

(18) Sadeghpour A, Alizadehasl A. The Right Ventricle: A Comprehensive Review from Anatomy, Physiology, and Mechanics to Hemodynamic, Functional, and Imaging Evaluation. Arch Cardiovasc Imaging. 2015; 3(4):e35717.

(19) Lee FA. Hemodynamics of the right ventricle in normal and disease states Cardiol Clin 1992;10(1):59-67.

(20) Petitjean C, Rougon N, Cluzel P. Assessment of myocardial function: a review of quantification methods and results using tagged MRI J Cardiovasc Magn Reson 2005;7(2):501-516.

(21) Ostenfeld E, Flachskampf FA. Assessment of right ventricular volumes and ejection fraction by echocardiography: from geometric approximations to realistic shapes Echo Res Pract 2015;2(1):R1-R11.

(22) Lang RM, Badano LP, Mor-Avi V, Afilalo J, Armstrong A, Ernande L, et al. Recommendations for cardiac chamber quantification by echocardiography in adults: an update from the American Society of Echocardiography and the European Association of Cardiovascular Imaging Eur Heart J Cardiovasc Imaging 2015;16(3):233-270

(23) Anavekar NS, Gerson D, Skali H, Kwong RY, Yucel EK, Solomon SD. Two-dimensional assessment of right ventricular function: an echocardiographic-MRI correlative study Echocardiography 2007;24(5):452-456.

(24) Verbraecken J, Van de Heyning P, De Backer W, Van Gaal L. Body surface area in normal-weight, overweight, and obese adults. A comparison study Metabolism 2006;55(4):515-524.

(25) Shors SM, Fung CW, Francois CJ, Finn JP, Fieno DS. Accurate quantification of right ventricular mass at MR imaging by using cine true fast imaging with steady-state precession: study in dogs Radiology 2004;230(2):383-388.

(26) Geva T. Is MRI the preferred method for evaluating right ventricular size and function in patients with congenital heart disease?: MRI is the preferred method for evaluating right ventricular size and function in patients with congenital heart disease Circ. Cardiovasc. Imaging 2014;7(1):190-197.

(27) Maffei E, Messalli G, Martini C, Nieman K, Catalano O, Rossi A, et al. Left and right ventricle assessment with Cardiac CT: validation study vs. Cardiac MR Eur Radiol 2012;22(5):1041-1049.

(28) Tadic M. Multimodality Evaluation of the Right Ventricle: An Updated Review Clin Cardiol 2015;38(12):770-776.

(29) Kochav J, Simprini L, Weinsaft JW. Imaging of the right heart--CT and CMR Echocardiography 2015;32 Suppl 1:S53-68.

(30) Alfakih K, Thiele H, Plein S, Bainbridge GJ, Ridgway JP, Sivananthan MU. Comparison of right ventricular volume measurement between segmented k-space gradient-echo and steady-state free precession magnetic resonance imaging J Magn Reson Imaging 2002;16(3):253-258.

(31) Sandstede J, Lipke C, Beer M, Hofmann S, Pabst T, Kenn W, et al. Age- and gender-specific differences in left and right ventricular cardiac function and mass determined by cine magnetic resonance imaging Eur Radiol 2000;10(3):438-442.

(32) Maceira AM, Prasad SK, Khan M, Pennell DJ. Reference right ventricular systolic and diastolic function normalized to age, gender and body surface area from steady-state free precession cardiovascular magnetic resonance Eur Heart J 2006;27(23):2879-2888.

(33) Foppa M, Arora G, Gona P, Ashrafi A, Salton CJ, Yeon SB, et al. Right Ventricular Volumes and Systolic Function by Cardiac Magnetic Resonance and the Impact of Sex, Age, and Obesity in a Longitudinally Followed Cohort Free of Pulmonary and Cardiovascular Disease: The Framingham Heart Study Circ Cardiovasc Imaging 2016;9(3):e003810.

(34) Aquaro GD, Camastra G, Monti L, Lombardi M, Pepe A, Castelletti S, et al. Reference values of cardiac volumes, dimensions, and new functional parameters by MR: A multicenter, multivendor study J Magn Reson Imaging 2017;45(4):1055-1067.

(35) Le Ven F, Bibeau K, De Larochelliere E, Tizon-Marcos H, Deneault-Bissonnette S, Pibarot P, et al. Cardiac morphology and function reference values derived from a large subset of healthy young Caucasian adults by magnetic resonance imaging Eur Heart J Cardiovasc Imaging 2016;17(9):981-990.

(36) Alfakih K, Plein S, Thiele H, Jones T, Ridgway JP, Sivananthan MU. Normal human left and right ventricular dimensions for MRI as assessed by turbo gradient echo and steady-state free precession imaging sequences J Magn Reson Imaging 2003;17(3):323-329.

(37) Clarke CJ, Gurka MJ, Norton PT, Kramer CM, Hoyer AW. Assessment of the accuracy and reproducibility of RV volume measurements by CMR in congenital heart disease JACC Cardiovasc Imaging 2012;5(1):28-37.

(38) James SH, Wald R, Wintersperger BJ, Jimenez-Juan L, Deva D, Crean AM, et al. Accuracy of right and left ventricular functional assessment by short-axis vs axial cine steady-state free-precession magnetic resonance imaging: intrapatient correlation with main pulmonary artery and ascending aorta phase-contrast flow measurements Can Assoc Radiol J 2013;64(3):213-219.

(39) Fratz S, Schuhbaeck A, Buchner C, Busch R, Meierhofer C, Martinoff S, et al. Comparison of accuracy of axial slices versus short-axis slices for measuring ventricular volumes by cardiac magnetic resonance in patients with corrected tetralogy of fallot Am J Cardiol 2009;103(12):1764-1769.

(40) Souto Bayarri M, Masip Capdevila L, Remuinan Pereira C, Suarez-Cuenca JJ, Martinez Monzonis A, Couto Perez MI, et al. Cardiac magnetic resonance analysis of right ventricular function: comparison of quantification in the short-axis and 4-chamber planes Radiologia 2015;57(1):50-55.

(41) Marchesseau S, Ho JX, Totman JJ. Influence of the short-axis cine acquisition protocol on the cardiac function evaluation: A reproducibility study Eur J Radiol Open 2016;3:60-66.

(42) Sievers B, Kirchberg S, Bakan A, Franken U, Trappe HJ. Impact of papillary muscles in ventricular volume and ejection fraction assessment by cardiovascular magnetic resonance J Cardiovasc Magn Reson 2004;6(1):9-16.

(43) Winter MM, Bernink FJ, Groenink M, Bouma BJ, van Dijk AP, Helbing WA, et al. Evaluating the systemic right ventricle by CMR: the importance of consistent and reproducible delineation of the cavity J Cardiovasc Magn Reson 2008;10:40-429X-10-40.

(44) Beerbaum P, Barth P, Kropf S, Sarikouch S, Kelter-Kloepping A, Franke D, et al. Cardiac function by MRI in congenital heart disease: impact of consensus training on inter-institutional variance J Magn Reson Imaging 2009;30(5):956-966.

(45) Helbing WA, Rebergen SA, Maliepaard C, Hansen B, Ottenkamp J, Reiber JH, et al. Quantification of right ventricular function with magnetic resonance imaging in children with normal hearts and with congenital heart disease Am Heart J 1995;130(4):828-837.

(46) Freling HG, van Wijk K, Jaspers K, Pieper PG, Vermeulen KM, van Swieten JM, et al. Impact of right ventricular endocardial trabeculae on volumes and function assessed by CMR in patients with tetralogy of Fallot Int J Cardiovasc Imaging 2013;29(3):625-631.

(47) Kawel-Boehm N, Maceira A, Valsangiacomo-Buechel ER, Vogel-Claussen J, Turkbey EB, Williams R, et al. Normal values for cardiovascular magnetic resonance in adults and children J Cardiovasc Magn Reson 2015;17:29-015-0111-7.

(48) Carlsson M, Ugander M, Heiberg E, Arheden H. The quantitative relationship between longitudinal and radial function in left, right, and total heart pumping in humans Am J Physiol Heart Circ Physiol 2007;293(1):H636-44.

(49) Rompel O, Janka R, May MS, Glockler M, Cesnjevar R, Dittrich S, et al. Cardiac MRI in Children and Adolescents Who Have Undergone Surgical Repair of Right-Sided Congenital Heart Disease: Automated Left Ventricular Volumes and Function Analysis and Effects of Different Manual Adjustments Rofo 2015;187(12):1099-1107.

(50) Effron B, Tibshirani RJ. An introduction to the bootstrap. Monographs on statistics and applied probability 1993;57:436.

(51) Hudsmith LE, Petersen SE, Francis JM, Robson MD, Neubauer S. Normal human left and right ventricular and left atrial dimensions using steady state free precession magnetic resonance imaging. J Cardiovasc Magn Reson. 2005;7(5):775-82.

(52) Mooij CF, de Wit CJ, Graham DA, Powell AJ, Geva T. Reproducibility of MRI measurements of right ventricular size and function in patients with normal and dilated ventricles. J Magn Reson Imaging. 2008;28(1):67-73.

(53) Matsuoka H, Hamada M, Honda T, Kobayashi T, Suzuki M, Ohtani T, Takezaki M, Abe M, Fujiwara Y, Sumimoto T, et al. Measurement of cardiac chamber volumes by cine magnetic resonance imaging. Angiology. 1993;44(4):321-7.

(54) Sakuma H, Kawada N, Kubo H, Nishide Y, Takano K, Kato N, Takeda K. Effect of breath holding on blood flow measurement using fast velocity encoded cine MRI. Magn Reson Med. 2001;45(2):346-8.

(55) Ferrigno M, Hickey DD, Linér MH, Lundgren CE. Cardiac performance in humans during breath holding. J Appl Physiol (1985). 1986;60(6):1871-7.

(56) Harer C. Einfluss der Definition der Basisebene auf die Normalwerte der Funktionsanalyse des linken Ventrikels in der Herz-MRT Diplomabeit Medizinische Universität Graz 2016.